

Article

# Investigation on Novel *E/Z* 2-Benzylideneindan-1-One-Based Photoswitches with AChE and MAO-B Dual Inhibitory Activity

Marco Paolino <sup>1,†</sup>, Modesto de Candia <sup>2,†</sup>, Rosa Purgatorio <sup>2</sup>, Marco Catto <sup>2</sup>, Mario Saletti <sup>1</sup>, Anna Rita Tondo <sup>2</sup>, Orazio Nicolotti <sup>2</sup>, Andrea Cappelli <sup>1</sup>, Antonella Brizzi <sup>1</sup>, Claudia Mugnaini <sup>1</sup>, Federico Corelli <sup>1</sup> and Cosimo D. Altomare <sup>2,\*</sup>

<sup>1</sup> Department of Biotechnology, Chemistry and Pharmacy, University of Siena, Via A. Moro 2, I-53100 Siena, Italy; paolino3@unisi.it (M.P.); mario.saletti2@unisi.it (M.S.); andrea.cappelli@unisi.it (A.C.); antonella.brizzi@unisi.it (A.B.); claudia.mugnaini@unisi.it (C.M.); federico.corelli@unisi.it (F.C.)

<sup>2</sup> Department of Pharmacy-Pharmaceutical Sciences, University of Bari Aldo Moro, Via E. Orabona 4, I-70125 Bari, Italy; modesto.decandia@uniba.it (M.d.C.); rosa.purgatorio@uniba.it (R.P.); marco.catto@uniba.it (M.C.); anna.tondo@uniba.it (A.R.T.); orazio.nicolotti@uniba.it (O.N.)

\* Correspondence: cosimodamiano.altomare@uniba.it

† These authors contributed equally to this work.

**Abstract:** The multitarget therapeutic strategy, as opposed to the more traditional ‘one disease-one target-one drug’, may hold promise in treating multifactorial neurodegenerative syndromes, such as Alzheimer’s disease (AD) and related dementias. Recently, combining a photopharmacology approach with the multitarget-directed ligand (MTDL) design strategy, we disclosed a novel donepezil-like compound, namely 2-(4-((diethylamino)methyl)benzylidene)-5-methoxy-2,3-dihydro-1*H*-inden-1-one (**1a**), which in the *E* isomeric form (and about tenfold less in the UV-B photo-induced isomer *Z*) showed the best activity as dual inhibitor of the AD-related targets acetylcholinesterase (AChE) and monoamine oxidase B (MAO-B). Herein, we investigated further photoisomerizable 2-benzylideneindan-1-one analogs **1b–h** with the unconjugated tertiary amino moiety bearing alkyls of different bulkiness and lipophilicity. For each compound, the thermal stable *E* geometric isomer, along with the *E/Z* mixture as produced by UV-B light irradiation in the photostationary state (PSS, 75% *Z*), was investigated for the inhibition of human ChEs and MAOs. The pure *E*-isomer of the *N*-benzyl(ethyl)amino analog **1h** achieved low nanomolar AChE and high nanomolar MAO-B inhibition potencies (IC<sub>50</sub>s 39 and 355 nM, respectively), whereas photoisomerization to the *Z* isomer (75% *Z* in the PSS mixture) resulted in a decrease (about 30%) of AChE inhibitory potency, and not in the MAO-B one. Molecular docking studies were performed to rationalize the different *E/Z* selectivity of **1h** toward the two target enzymes.

**Keywords:** neurodegenerative diseases; cholinesterase inhibitors; monoaminoxidase inhibitors; photopharmacology



**Citation:** Paolino, M.; de Candia, M.; Purgatorio, R.; Catto, M.; Saletti, M.; Tondo, A.R.; Nicolotti, O.; Cappelli, A.; Brizzi, A.; Mugnaini, C.; et al. Investigation on Novel *E/Z* 2-Benzylideneindan-1-One-Based Photoswitches with AChE and MAO-B Dual Inhibitory Activity. *Molecules* **2023**, *28*, 5857. <https://doi.org/10.3390/molecules28155857>

Academic Editor: Alejandro Samhan-Arias

Received: 25 June 2023

Revised: 22 July 2023

Accepted: 26 July 2023

Published: 3 August 2023



**Copyright:** © 2023 by the authors. Licensee MDPI, Basel, Switzerland. This article is an open access article distributed under the terms and conditions of the Creative Commons Attribution (CC BY) license (<https://creativecommons.org/licenses/by/4.0/>).

## 1. Introduction

The incidence of neurodegenerative diseases in the aging world population, particularly Alzheimer’s disease (AD) and Parkinson’s disease (PD), is influenced by the increase in average life expectancy and unregulated lifestyle, as highlighted in the recent World Alzheimer Reports [1]. In the absence of disease-modifying drugs, AD and PD are considered incurable, and this serious health threat is expected to increase in the near future [2]. By limiting oxidative stress and the associated inflammatory state, as well as by fine-tuning the concentration of neurotransmitters, it is possible to apply some palliative pharmacological therapies to slow down the progression of neurodegenerative diseases and control their symptoms. Among the various pharmacological targets identified, monoamine oxidases (MAOs) and cholinesterases (ChEs) are of particular interest.

MAOs are mitochondrial enzymes responsible for the oxidative catabolism of endogenous monoamines and xenobiotics. Their levels increase with age, resulting in increased production of reactive oxygen species (ROS) as by-products of the oxidation process, which ultimately leads to neuroinflammation and subsequent brain tissue damage. In humans, two enzyme isoforms, MAOs A and B, have been identified [3], both playing roles in the inactivation of endogenous monoaminergic neurotransmitters, albeit with different specificities. MAO-A is mainly responsible for the catabolism of norepinephrine, serotonin, and epinephrine, whereas MAO-B is more selective for tyramine and dopamine [4,5]. Selective MAO-B inhibitors (MAO-B Is) showed neuroprotective effects due to a reduction in ROS formation and improved cognitive abilities in patients with neurodegenerative disorders by enhancing the level of monoamine neurotransmitters in the CNS [6]. The MAO-B Is selegiline, safinamide, and rasagiline, whose structure is incorporated into that of ladostigil (Figure 1), are used for the treatment of PD [7].

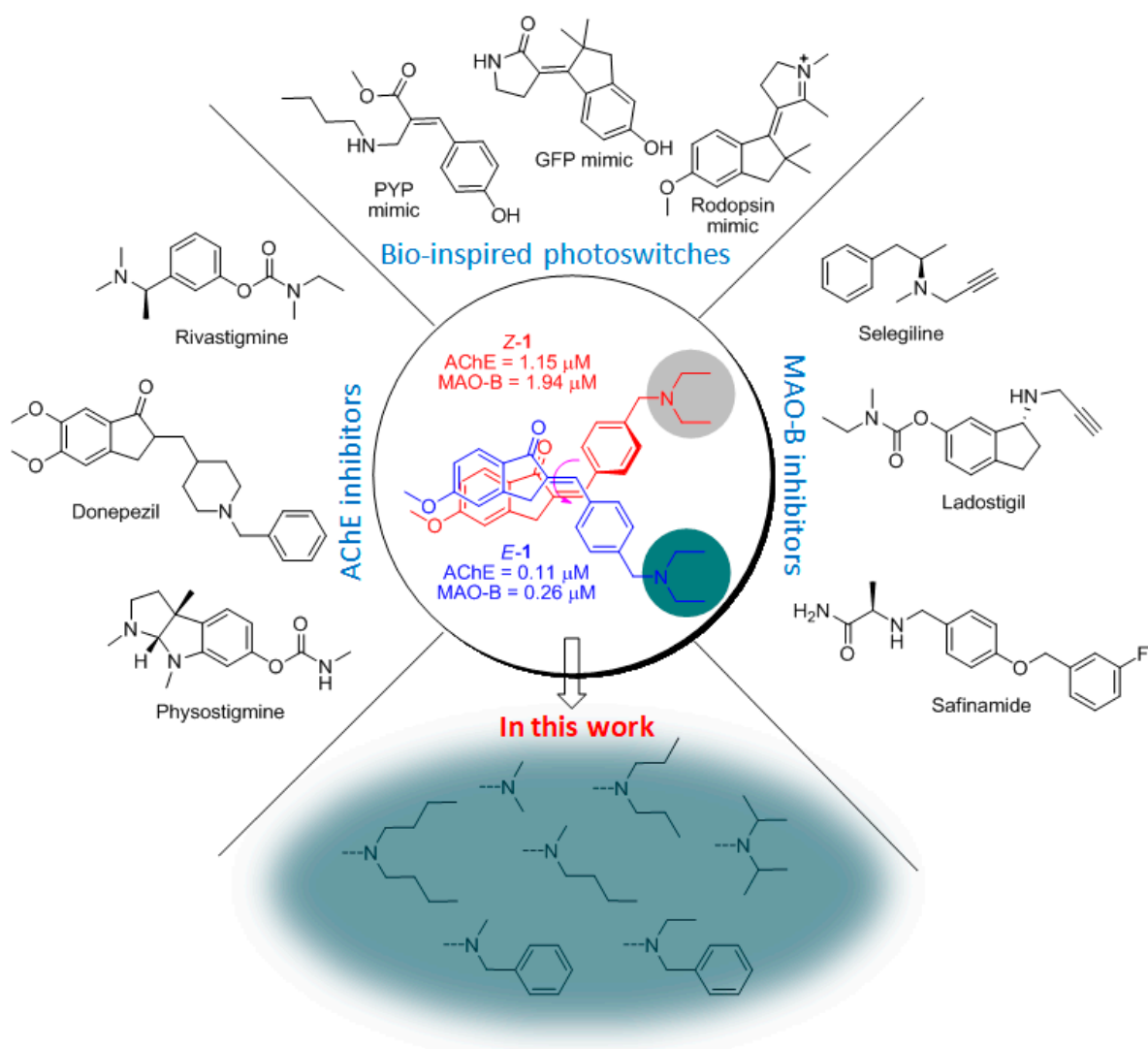


**Figure 1.** Photoisomerizable dual AChE/MAO-B inhibitors synthesized in this study aim at optimizing the tertiary amino head of the hit compound **1a**; the *E/Z* isomers of **1a** are surrounded by known AChE-Is, MAO-B-Is, and synthetic light-gated molecular switches and rotors.

Cholinesterase exists in two isoforms, acetylcholinesterase (AChE) and butyrylcholinesterase (BChE), which catalyze the hydrolysis of acetylcholine (ACh), that activates cholinergic synapses and receptors [8]. The impairment of cholinergic neurotransmission is a downstream process in the cognitive deficit associated with AD. To date, cholinesterase inhibitors (ChE Is) are among

the few approved drugs for the symptomatic treatment of AD (Figure 1) that are able to restore cortical cholinergic neurotransmission with consequent beneficial effects on cognition in both AD and PD-related dementia [9]. Among them, rivastigmine, donepezil, and galantamine are currently indicated in patients with mild-to-moderate AD [10,11].

Due to the multifactorial nature of AD, as well as the frequent comorbidity of various neurodegenerative diseases, the design and optimization of multitarget-directed ligands (MTDLs) represents a noteworthy pharmaceutical development strategy [12–16]. In particular, compounds targeting AChE and MAO-B could be useful tools for the treatment of neurodegenerative diseases. The first concrete result was achieved with ladostigil (Figure 1), a dual inhibitor of AChE (reversible) and MAO-B (irreversible), currently in clinical trials (NCT01354691) as an anti-AD drug [17].

Because of the extreme individual variability of the neurodegenerative processes during the different stages of the disease, the search for innovative pharmacological tools that can be used in precision medicine is a real challenge. Controlling the activity of a drug by appropriate external stimuli could represent an effective strategy in the development of “individualizable molecules”. Among the external stimuli, there is growing interest in light, which can affect a tissue with high spatial and temporal precision in a noninvasive and easily controlled manner [18].

In the last decade, the concept of photopharmacology has been widely developed using bioactive molecules that can change their biological effect as a result of light irradiation [18]. In the initial phase, the development of photoactive molecules was based on photolabile functional groups that irreversibly detached from the photodrug and released the bioactive molecule into the irradiated area. Later, with the advent of light-controlled molecular switches (notably azobenzene) aimed at developing more adaptable molecules, photodrug design shifted to the conjugation of bioactive molecules with molecular photoswitches that could change their geometry in response to an appropriate light stimulus and thus, reversibly switch the pharmacological activity on or off [19–21].

Several case studies have been proposed for molecules with photomodulable activity against targets such as ion channels [22–24], enzymes [25,26], and G-protein-coupled receptors (GPCRs) [19,21,27]. However, despite the crucial role of AChE and MAO-B in the neuronal network, which proceeds with extremely fast kinetics, there are few examples of photomodulable inhibitors for these enzymes [28,29].

In this context, we have combined the expertise in the synthesis and characterization of biomimetic light-controlled molecular switches and motors [30–36] and in the design of ChE-Is [37–39], which have recently led to a small series of photoisomerizable donepezil-like compounds with on-off inhibitory activity towards AChE and MAO-B [40]. These molecules consist of a diversely decorated indanone moiety linked to an N-benzyl-N-ethylethanamine group via an isomerizable carbon-carbon double bond. Their irradiation leads to the spatial repositioning of the key pharmacophore features responsible for the interactions in the binding sites of the target enzymes.

Among these molecules, **1a** (Figure 1), bearing the 5-methoxyindan-1-one moiety, showed the most interesting combination of photophysical and biological profiles. The geometric isomer *E*-**1a** achieved noteworthy inhibitory activity in the high nanomolar range against both enzymes (AChE  $IC_{50} = 0.113 \mu\text{M}$ , MAO-B  $IC_{50} = 0.260 \mu\text{M}$ ), showing selectivity over the BChE and MAO-A isoforms of two orders of magnitude. Irradiation of *E*-**1a** with UV-B light produced an *E/Z* mixture composed of 75% of the *Z*-isomer in the photostationary state (PSS), and the inhibitory effect of *Z*-**1a** on both AChE and MAO-B decreased by one order of magnitude (AChE  $IC_{50} = 1.15 \mu\text{M}$ , MAO-B  $IC_{50} = 1.94 \mu\text{M}$ ), demonstrating off-activity behavior.

Based on these findings, we expand herein the series of 5-methoxyindanone derivatives by synthesizing new compounds in which the tertiary amino residue of **1a** bears alkyls with different bulkiness and lipophilicity (Figure 1). A major aim of this study is the investigation of the effect of the amino/ammonium head on the diastereoisomerism-dependent activity

by evaluating the difference in the inhibitory capacity of the mixtures at the PSS, which mainly consists of the photoinduced isomer Z (75%), on AChE and MAO-B.

## 2. Design and Synthesis

From a pharmacological point of view, the structure of parent compound **1a** can be traced back to the well-known anti-Alzheimer drug donepezil. This molecule has a 5,6-methoxyindanone unit linked to an N-benzylpiperidine moiety via a chiral center. By manipulating this structure, Sheng and coworkers discovered non-chiral compounds with AChE-inhibitory activity comparable to donepezil [41]. Specifically, they replaced the chiral center with an exocyclic double bond and reversed the position of the benzyl ring with the basic center (e.g., compound **2**, Figure 2). In our previous study, focusing on dual AChE/MAO-B inhibitors, the effect of methoxy groups on the interaction with the two enzymes was investigated. We found that removing the 6-OMe group of the indanone moiety resulted in a molecule with submicromolar inhibitory activity for both target enzymes [40]. Thanks to the presence of the hemiindigoid chromophore [42,43], this molecule is able to reversibly photoisomerize by the application of UV light and spatially shift the functional groups responsible for the interaction in the binding sites of the two enzymes. Among the key pharmacophore features, the tertiary amino residue plays a first-rate role by interacting at the catalytic anionic site (CAS) site of AChE, anchoring the inhibitor in the enzyme gorge. Photoisomerization of the exocyclic double bond leads to the displacement of the indanone carbonyl, and the 5-OMe group alters their interactions in the middle of the binding gorge and at the peripheral anionic site (PAS).

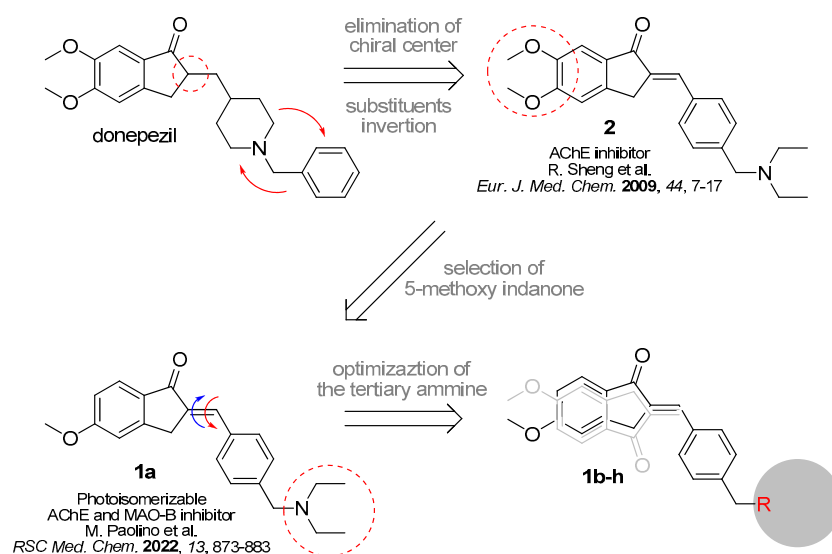
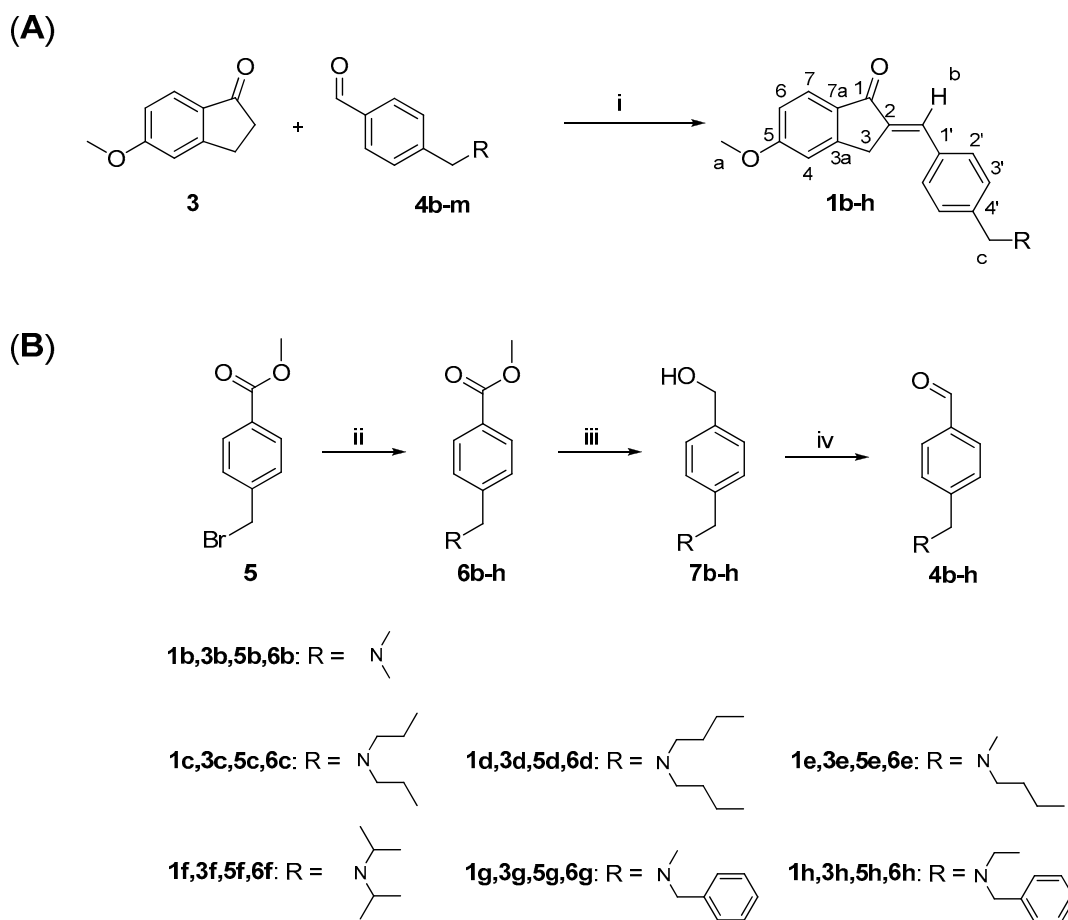


**Figure 2.** Design of the new photoisomerizable dual AChE/MAO-B inhibitors. Compounds **2** and **1a** have been reported in ref [41] and [40] respectively.

In this study, the ethyl residues on the tertiary amine were replaced by various alkyl chains (linear or branched) of different lipophilicity and bulkiness. These substitutions could have favorable or unfavorable effects on the interaction of the tertiary amine in the CAS region of the AChE gorge and, conversely, on other interactions in the middle gorge and in PAS. On the other hand, the increase in lipophilicity around the basic head could improve the inhibition potency against the MAO-B enzyme.

Compounds **1b–h** were prepared by aldol condensation of 5-methoxyindan-1-one (**3**) with the corresponding aldehyde derivative **4b–h** using KOH in methanol, as shown in Scheme 1A. In this reaction, only the *E* diastereoisomer was obtained for each compound, according to the assignment by  $^1\text{H}$  NMR analysis. In the  $^1\text{H}$  NMR spectra of compounds **1b–h**, the vinyl proton "b" (see Scheme 1A for numbering) shows a chemical shift of

7.5 ppm, consistent with the deshielding effect of the carbonyl group, as already observed in the spectrum of **1a**.



**Scheme 1.** Synthesis of compounds *E*-**1b–h** (A) and aldehyde derivatives **4b–h** (B). **Reagents and conditions:** (i) CH<sub>3</sub>OH, KOH, r.t., 2–6 h; (ii) appropriate secondary amine, CH<sub>2</sub>Cl<sub>2</sub>, reflux, 4–5 h; (iii) LiAlH<sub>4</sub>, dry THF, 12 h; (iv) MnO<sub>2</sub>, 1,4 dioxane, reflux, 2–4 h.

The aldehyde derivatives **4b–h** were synthesized according to the reactions shown in Scheme 1B. Bromide derivative **5** was reacted with the corresponding secondary amine in DCM at a refluxing temperature. The ester function of the resulting tertiary amines **6b–h** was reduced with LiAlH<sub>4</sub> in anhydrous THF to afford the primary alcohol derivatives **7b–h**, which were oxidized to the corresponding aldehydes **4b–h** with MnO<sub>2</sub> in refluxing 1,4-dioxane.

### 3. Photophysical and Photochemical Characterization

The substitutions at the amino group in compounds **1b–h** do not change the structure of the chromophore compared to their precursor **1a**. The absorption spectra registered in methanol at concentrations of about  $1 \times 10^{-5}$  M (Figure 3A and S40A in Supplementary Information) are indeed very similar to the UV-vis spectrum of **1a** [40]. For each compound, the absorption spectrum is dominated by an intense peak at about 334–340 nm (with an absorption tail up to about 390 nm) that largely overlaps with the emission spectrum from UV-B lamps. Therefore, this light emission was used for the photoisomerization of the new compounds in <sup>1</sup>H NMR and UV-Vis absorption experiments.

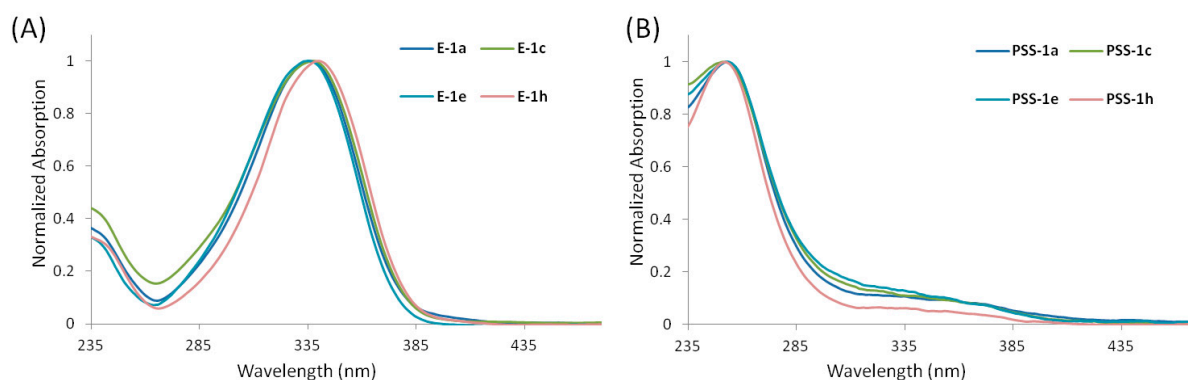


**Figure 3.** (A) Normalized UV-Vis absorption spectra of methanolic solutions of compounds *E*-1a,c,e,h. (B) Normalized UV-Vis absorption spectra of methanolic solution of compound 1a,c,e,h at PSS generated by UV-B irradiation.

Using  $^1\text{H}$  NMR spectroscopy, the formation of the *Z* diastereoisomer can be determined with confidence. Specifically, as previously done for 1a, methanol- $\text{d}_4$  solutions of compounds 1b–e at a concentration of about 10 mM were irradiated with UV-B light in a Pyrex NMR tube and observed until the photostationary state (PSS) was reached.

The same procedure was followed for compounds 1f–h. However, due to the poor solubility in methanol at the concentrations required for  $^1\text{H}$  NMR analysis, 1f–h was irradiated and monitored in an acetone- $\text{d}_6$  solution. The diastereomeric *E/Z* ratio of the obtained PSS-1b–h was determined by calculating the area of the easily distinguishable signals assigned to the *E* and *Z* isomers (Figure 4).

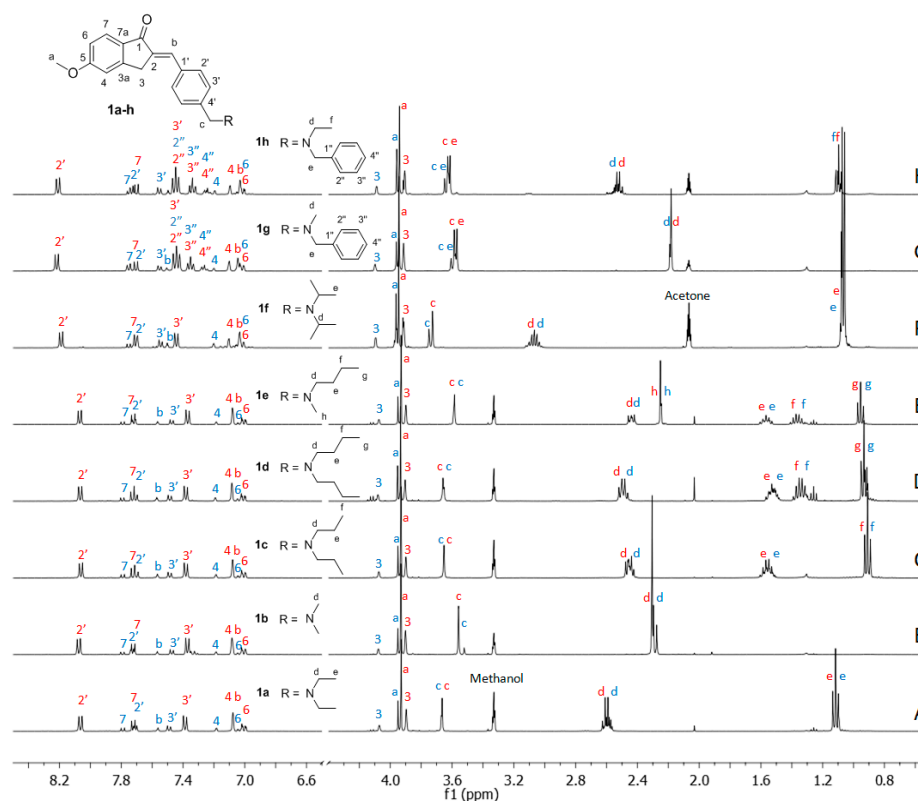


**Figure 4.**  $^1\text{H}$  NMR spectra (400 MHz) of the *E/Z* mixtures obtained at the PSSs after irradiation with UV-B light of compounds 1a–e (spectra A–E) in methanol- $\text{d}_4$  and of compounds 1f–h (spectra F–H) in acetone- $\text{d}_6$ . Blue numbering was used for assignment of the *E* diastereomers, while red numbering was used for the *Z* isomers.

In all experiments, the PSS resulting from UV-B irradiation consisted mainly of the *Z* geometric isomer (75%) together with the *E* isomer (25%), confirming that the replacement of the nonconjugated amino group by the hemiindigoid chromophore did not affect the photochemical properties of the new compounds.

As an example, Figure 5 shows the photoconversion kinetics obtained by irradiating **1c** (10 mM in methanol- $d_6$ ) in a Pyrex NMR tube using a multi-ray chamber equipped with two lamps (15 Watt GT15T8 Hg UV-B tube) at a temperature of 24 °C in continuous rotation. The solution was irradiated with UV-B light until reaching the PSS<sub>UV-B</sub> (almost completed in 50–80 min). Subsequently, the PSS<sub>UV-B</sub> solution was irradiated under the same conditions with UV-C light generated using two lamps (15 Watt GT15T8 Hg UV-C tube), observing the photoconversion of the *cis* isomer into the *trans* isomer without the appearance of photodegradation.

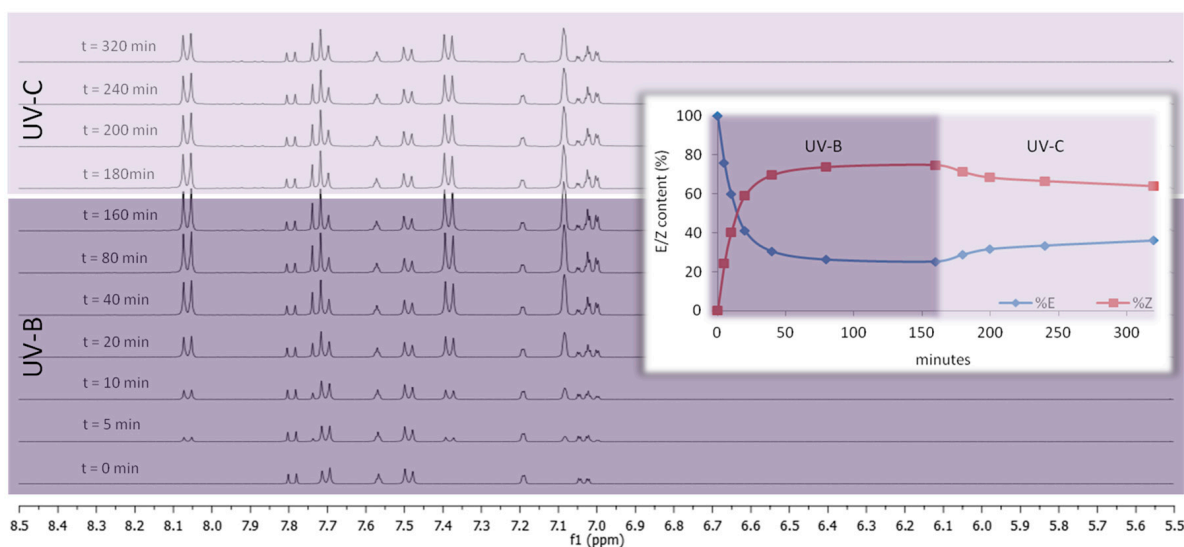


**Figure 5.** Comparison of the  $^1\text{H}$  NMR spectra (400 MHz,  $\text{CD}_3\text{OD}$ , range 8.5–5.5 ppm) recorded for monitoring the photoconversion kinetics of compound **1c** (concentration 10 mM). The methanolic solution was irradiated in a Pyrex NMR tube with UV-B light using a multi-ray chamber equipped with two tubular lamps (15 Watt GT15T8 Hg UV-B tube) at a temperature of 24 °C in continuous rotation for 160 min and, then for 160 min with UV-C light generated using two tubular lamps (15 Watt GT15T8 Hg UV-C tube).

All PSS-**1b–h** solutions were stored at room temperature in the dark (or even in visible ambient light) for 2 days and reexamined by  $^1\text{H}$  NMR. As with **Z-1a**, for which a half-life in MeOH at room temperature of 47 days was calculated [40], no significant change in *E/Z* composition was observed.

The effect of UV-B irradiation was also monitored by UV-Vis absorption spectroscopy (Figure 3B and S40B in Supplementary Information). Methanolic solutions ( $1 \times 10^{-5}$  M) of **1b–h** at the PSS showed a drastic decrease in the absorption bands attributed to the *E* diastereomers and the appearance of new blue-shifted absorption bands attributed to the presence of the *Z* diastereoisomers, consistent with a decrease in  $\pi$ - $\pi$  electron conjugation [44].

#### 4. Biological Evaluation

The pure *E* isomers **1b–h**, along with *E-1a* retested in this study, and the related *E/Z* mixtures at the PSS (75% *Z* isomer) were evaluated for their inhibitory activity against AChE and BChE, and MAO-A and B. The inhibition data summarized in Table 1 show that all compounds, without any noteworthy structure-dependent difference, are selective toward AChE and MAO-B over BChE and MAO-A, respectively.

**Table 1.** Inhibition data of recombinant human cholinesterases (AChE and BChE) and monoamine oxidases (MAOs A and B) by *E* isomers and *E/Z* mixtures of compounds **1a–h**.

Cmpds <sup>a</sup>	IC <sub>50</sub> (μM) or % Inhibition at 10 μM <sup>b</sup>			
	AChE <sup>c</sup>	BChE <sup>c</sup>	MAO-A <sup>c</sup>	MAO-B <sup>c</sup>
<i>E</i> - <b>1a</b>	0.105 ± 0.005 <sup>f</sup>	10.0 ± 0.15 <sup>f</sup>	(33 ± 3) <sup>f</sup>	0.260 ± 0.012 <sup>f</sup>
<i>E/Z</i> - <b>1a</b>	0.780 ± 0.013 <sup>f</sup>	(28 ± 6%) <sup>f</sup>	(45 ± 5) <sup>f</sup>	1.59 ± 0.04 <sup>f</sup>
<i>E</i> - <b>1b</b>	0.155 ± 0.010	n.a.	(33 ± 1)	0.686 ± 0.059
<i>E/Z</i> - <b>1b</b>	0.915 ± 0.138	(25 ± 10%)	(32 ± 2)	0.839 ± 0.123
<i>E</i> - <b>1c</b>	0.174 ± 0.017	(28 ± 7%)	(15 ± 1)	0.479 ± 0.081
<i>E/Z</i> - <b>1c</b>	0.295 ± 0.045	(20 ± 7%)	2.98 ± 0.08	0.743 ± 0.048
<i>E</i> - <b>1d</b>	0.990 ± 0.050	(28 ± 9%)	(12 ± 4)	0.338 ± 0.036
<i>E/Z</i> - <b>1d</b>	2.28 ± 0.21	n.a.	(37 ± 2)	0.382 ± 0.006
<i>E</i> - <b>1e</b>	0.102 ± 0.019	5.00 ± 0.45	(20 ± 5)	0.178 ± 0.086
<i>E/Z</i> - <b>1e</b>	1.36 ± 0.06	n.a.	(25 ± 5)	0.651 ± 0.061
<i>E</i> - <b>1f</b>	0.261 ± 0.014	10.0 ± 0.85	(22 ± 2)	0.178 ± 0.086
<i>E/Z</i> - <b>1f</b>	1.41 ± 0.09	(20 ± 3%)	3.19 ± 0.10	0.241 ± 0.026
<i>E</i> - <b>1g</b>	0.115 ± 0.004	9.90 ± 0.11	(39 ± 7)	0.292 ± 0.060
<i>E/Z</i> - <b>1g</b>	0.135 ± 0.062	(40 ± 2%)	(49 ± 1)	0.354 ± 0.070
<i>E</i> - <b>1h</b>	0.039 ± 0.001	7.00 ± 0.01	(13 ± 6)	0.355 ± 0.134
<i>E/Z</i> - <b>1h</b>	0.053 ± 0.006	10.0 ± 0.32	(39 ± 5)	0.358 ± 0.008
Donepezil <sup>d</sup>	0.021 ± 0.005	4.80 ± 1.00		
Tacrine <sup>d</sup>	0.090 ± 0.005	0.025 ± 0.003		
Clorgiline <sup>e</sup>			0.0022 ± 0.0002	2.48 ± 0.43
Safinamide <sup>e</sup>			(18 ± 3)	0.028 ± 0.001

<sup>a</sup> The diastereomeric *E/Z* mixtures' ratios (25:75) at the photostationary state after UV-B light irradiation of the *E* methanolic solutions were established for all compounds by <sup>1</sup>H NMR spectrometry. <sup>b</sup> IC<sub>50</sub> values determined by interpolation of the sigmoidal dose–response curves as obtained by regression with GraphPad Prism software (ver.5.01) of at least seven data points, or percent inhibition in parentheses for samples achieving less than 50% inhibition at 10 μM concentration; n.a. = not active; data are means ± SD of three independent measurements. <sup>c</sup> Human cholinesterases and monoamine oxidase isoforms. <sup>d</sup> donepezil and tacrine were used as positive controls in AChE and BChE inhibition assays, respectively. <sup>e</sup> Clorgiline and safinamide were used as positive controls in MAO-A and MAO-B inhibition assays, respectively. <sup>f</sup> Data re-determined in this work, agreeing with those previously reported.

ChE inhibitory activities were determined by applying Ellman's assay with slight modifications, using the drugs donepezil and tacrine as positive controls of AChE and BChE selective inhibition, respectively [45,46]. All the pure geometric isomers *E*-**1a–h** selectively inhibit AChE, with IC<sub>50</sub> values falling in the submicromolar concentration range. Weaker inhibition of BChE was observed for all the compounds, with only *E*-**1f–h** achieving finite IC<sub>50</sub>s ≤ 10 μM. *E*-**1h** (IC<sub>50</sub> = 39 nM) turned out almost equipotent with donepezil (IC<sub>50</sub> = 21 nM), taken as positive control together with the dual AChE/BChE inhibitor tacrine. All the *E/Z* mixtures (75% *Z*) were found to be less active toward AChE than the corresponding pure *E* isomers, suggesting that the *Z* isomers have a lower binding affinity compared to the *E* isomers, as previously observed for the pure *Z*-**1a** [40].

A pairwise comparison of the AChE inhibition data with the physicochemical features of the tertiary amino head would suggest that the hydrophobicity/bulkiness (not sharply distinguishable within this series) of the -NR<sub>2</sub> may affect the AChE inhibitory potency of the examined compounds. However, the pure *E* isomers cover an IC<sub>50</sub> range of just 1.4 log units, and with the exception of the most active (**1h**, R = -N(Et)Bn) and the least active (**1d**, R = -N<sup>n</sup>Bu<sub>2</sub>) inhibitors, the activity data for the other six compounds span a range of only 0.5 log units. Nevertheless, within the limits of the biological and lipophilicity space explored, a nonlinear (likely parabolic) correlation trend (not shown) between -logIC<sub>50</sub> and the calculated log P for the -NR<sub>2</sub> fragment appears to hold for six of eight compounds. Two apparent outliers with respect to the parabolic relationship trend were the less-active-than-predicted **1f** (likely, higher steric hindrance of <sup>i</sup>Pr compared to <sup>n</sup>Pr groups in **1c**) and the more-active-than-predicted **1h** (additional aromatic interactions of the Bn group compared to Et in **1a**).



The mechanism of AChE inhibition by the most potent inhibitor *E-1h*, was investigated. Lineweaver–Burk curves were generated with a fixed amount of AChE and substrate concentrations ranging between 25 and 300  $\mu\text{M}$  in the absence or presence of the inhibitor at different concentrations (ranging from 5 to 500 nM). The binding of *E-1h* to AChE changed both  $V_{max}$  and  $K_m$  values, a trend generally attributed to the mixed-type inhibition (Figure 6). The replot of the slopes versus the corresponding inhibitor concentrations provided a  $K_i$  value of 100 nM.

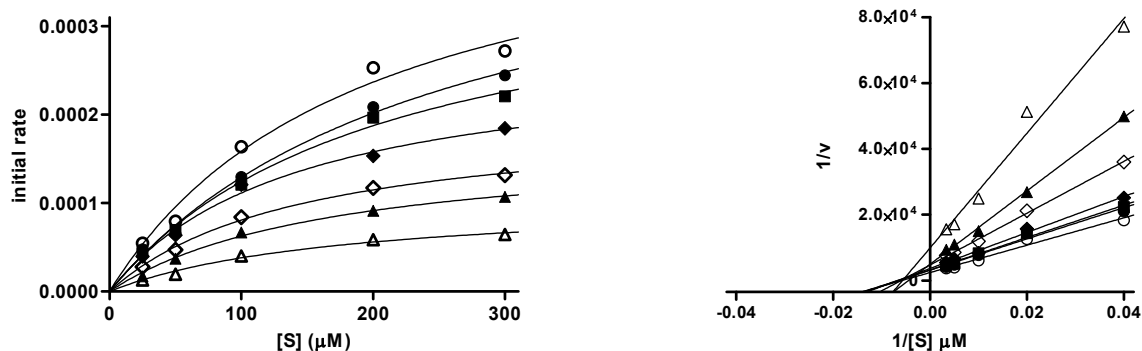


**Figure 6.** Inhibition kinetics (left) and Lineweaver–Burk plot (right),  $r^2 = 0.983$ – $0.999$  for hAChE (0.2 U/mL) and *E-1h* (0–500 nM), using different substrate (acetylthiocholine iodide) concentrations (50–300  $\mu\text{M}$ ). The replot ( $r^2 = 0.997$ ) of the slopes versus [I] determined the  $K_i$  (100 nM) as the x-axis intercept (see Supplementary Information). ( $\circ$ ) no inhibitor, ( $\bullet$ ) 10 nM, ( $\blacksquare$ ) 25 nM, ( $\blacklozenge$ ) 50 nM, ( $\diamond$ ) 100 nM, ( $\blacktriangle$ ) 200 nM, ( $\triangle$ ) 500 nM.

Taking into account our previous findings [40] and literature data on structurally similar compounds [47,48], MAO-A/B inhibition was evaluated for pure *E* isomers and *E/Z* mixtures. All the compounds in the pure *E* form proved to be MAO-B-selective inhibitors with all submicromolar  $\text{IC}_{50}$  values. Only in two cases, namely *E/Z* **1c** ( $R = -\text{N}^{\text{ipr}}\text{Pr}_2$ ) and **1f** ( $R = -\text{N}^{\text{ipr}}\text{Pr}_2$ ), finite  $\text{IC}_{50}$  values around 3  $\mu\text{M}$  were achieved against MAO-A, with the *Z* isomers being slightly more potent than the *E* isomers.

The  $\text{IC}_{50}$  values of MAO-B are in a narrow concentration range (just 0.6 log units) with no apparent lipophilicity-dependent effect. Even in the case of MAO-B inhibition, the *Z* isomers were found to be less potent than the *E* isomers, with the notable exception of **1h** ( $R = -\text{N}(\text{Et})\text{Bn}$ ) whose *E/Z* mixture in the PSS (75% *Z*) achieving the same  $\text{IC}_{50}$  as the pure *E-1h*.

Combining the inhibition data on the two enzymes, it is interesting to note that the replacement of the  $-\text{NEt}_2$  group of compound **1a** with a more hindered dissymmetrical substituent as in the case of compound **1e** ( $R = -\text{N}(\text{Me})\text{Bu}$ ) led to an improvement in the MAO-B  $\text{IC}_{50}$  of the diastereoisomer *E* ( $\text{IC}_{50}$  *E-1a* = 0.260  $\mu\text{M}$  vs. *E-1e* = 0.178  $\mu\text{M}$ ) at the expense of the diastereoisomeric difference ( $\text{IC}_{50}$  PSS *E/Z-1a* = 1.59  $\mu\text{M}$  vs. PSS *E/Z-1e* 0.651  $\mu\text{M}$ ). In contrast, the inhibitory capacity of *E-1e* towards AChE remained almost unchanged with respect to **1a** while significantly increasing the deactivating effect of light ( $\text{IC}_{50}$  PSS *E/Z-1a* = 0.78  $\mu\text{M}$  vs. PSS *E/Z-1e* 1.36  $\mu\text{M}$ ).

Regarding the potent AChE/MAO-B dual inhibitor **1h**, the *E* isomer is slightly more potent than the *Z* isomer as an AChE inhibitor, whereas no diastereoselectivity was observed for MAO-B inhibition.

## 5. Molecular Docking Analysis

To explain the observed inhibition data of the isomers *E-1h* and *Z-1h* against human AChE and MAO-B at the molecular level, docking calculations were performed on crystal structures of hAChE complexed with donepezil (PDB code: 4EY7) and hMAO-B in complex with safinamide (PDB code: 2V5Z). Considering the top-scored docking pose, both *E-1h* and *Z-1h* diastereoisomers accommodate in the gorge of the active site, in the middle of the PAS and the CAS [49].

In particular, the indanone group of *E*-**1h**, in its top-scored pose (Figure 7), occupies the PAS by establishing a  $\pi$ - $\pi$  interaction with W286 and the gorge through a backbone H-bond with F295 mediated by the carbonyl group; additionally, it interacts inside the CAS forming a cation- $\pi$  interaction, which involves W86 and the protonated tertiary amino group. Otherwise, the **1h** in *Z* geometry locates the indanone core away from the PAS and contacts the CAS through  $\pi$ - $\pi$  interactions with W86; moreover, the *Z*-isomer engages the aromatic residues of the gorge, and, more specifically, Y341 and Y337 by  $\pi$ - $\pi$  stacking and cation- $\pi$  interactions, respectively. More importantly, the docking-based comparison of *E* and *Z* geometries shows that the former best complies with the X-ray donepezil bioactive conformation (Figure 8). The indanone cores of donepezil and *E*-**1h** are well superimposed, and both make interactions with F295 and W286. Furthermore, although lacking the piperidine nitrogen as donepezil, which forms cation- $\pi$  interaction with Y337, *E*-**1h** has a protonable benzylamino group which may engage double cation- $\pi$  interactions with W86, as the cation- $\pi$  interaction and  $\pi$ - $\pi$  stacking found out in the AChE inhibitor drug. Noteworthy, the higher inhibitor potency of the *E*-**1h** diastereoisomer is in agreement with its higher docking score and ligand efficiency (LE) values.

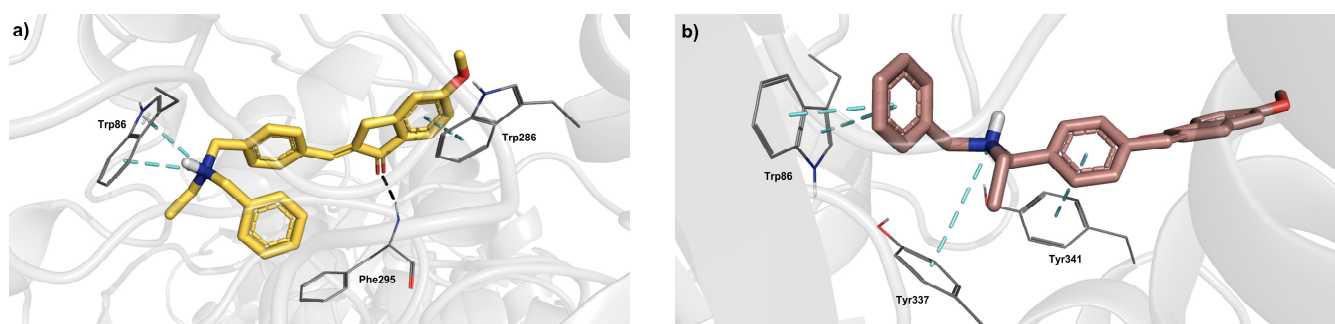


**Figure 7.** Glide top-ranked docking poses of (a) *E*-**1h** (docking score =  $-13.172$  kcal/mol, ligand efficiency =  $-0.439$ ) and (b) *Z*-**1h** (docking score =  $-11.494$  kcal/mol, ligand efficiency =  $-0.383$ ) in complex with hAChE (PDB 4EY7; donepezil: docking score =  $-13.117$  kcal/mol, ligand efficiency =  $-0.468$ ). The diastereoisomer ligands are depicted as sticks; the interacting residues are rendered as lines, while protein is represented as a cartoon. Dashed black lines represent H-bond; meanwhile,  $\pi$ - $\pi$  and  $\pi$ -cation interactions are indicated by dashed cyan lines.

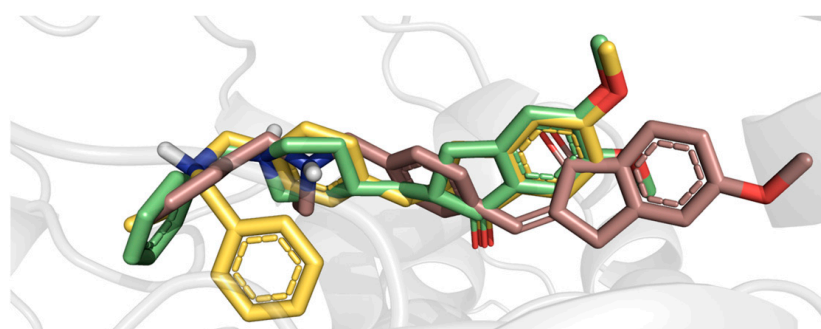


**Figure 8.** Superimposition of *E*-**1h** (yellow sticks), *Z*-**1h** (violet sticks), and donepezil (green sticks) as docked in the top-scored poses (*E/Z*-**1h**) or established by the X-ray crystal structure (donepezil) within the AChE binding site.

As far as docking calculation on hMAO-B is concerned, the top-scored poses of both *E*-**1h** and *Z*-**1h** diastereoisomers show the indanone moiety facing the FAD moiety (Figure 9). As experienced by the cognate ligand, an H-bond is established between the carbonyl backbone of I199 and the protonated amino, as well as  $\pi$ - $\pi$  stacking interactions.

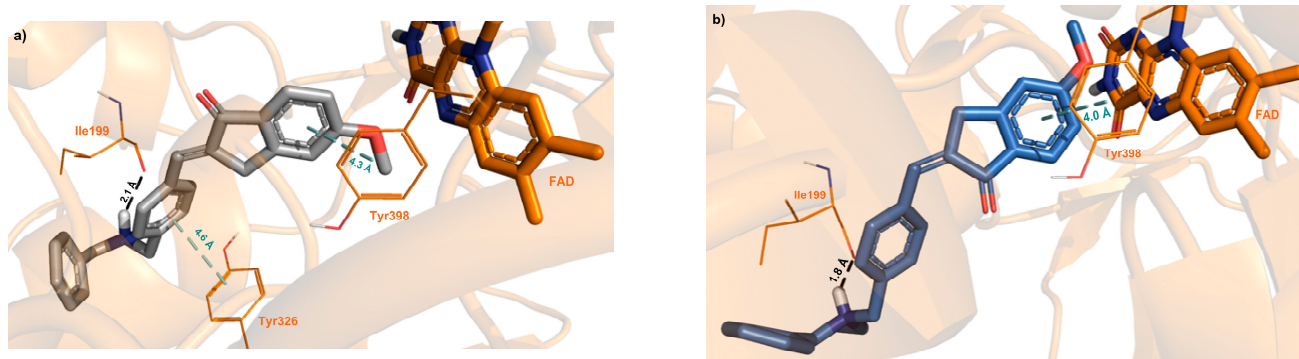


**Figure 9.** Glide top-ranked docking poses of (a) *E*-**1h** (grey stick, docking score =  $-10.129$  kcal/mol, ligand efficiency =  $-0.338$ ) and (b) *Z*-**1h** (blue stick, docking score =  $-12.256$  kcal/mol, ligand efficiency =  $-0.409$ ) in complex with hMAO-B (PDB 2V5Z; safinamide: docking score =  $-10.428$  kcal/mol, ligand efficiency =  $-0.474$ ). The diastereoisomer ligands are depicted as sticks; the interacting residues are rendered as lines, while protein is represented as cartoons. Dashed black lines represent H-bonds; meanwhile,  $\pi$ - $\pi$  and  $\pi$ -cation interactions are represented as dashed cyan lines. FAD coenzyme is shown in orange sticks.

Unlike safinamide, the indanone scaffold achieves  $\pi$ - $\pi$  interaction with Y398 for both the *E* and *Z* isomers, while the conjugated benzyl group engages Y326, an MAO-B selective residue [50] only in the *E* form. In the case of the top-scored docking poses of **1h** complexed with MAO-B, the Glide docking score and the calculated ligand efficiency slightly favors the *Z* isomer over the *E* isomer, likely agreeing with the experimental  $IC_{50}$  values, considering that even the PSS *E/Z* mixture containing 75% *Z* isomer showed a similar inhibition potency of the pure *E* isomer.

## 6. Materials and Methods

**Synthesis.** All chemicals used were of reagent grade. Yields refer to purified products and are not optimized. Merck silica gel 60 (230–400 mesh) was used for column chromatography. Merck TLC plates and silica gel 60 F254 were used for TLC. NMR spectra were obtained with a Bruker 400 AVANCE spectrometer in the indicated solvents. Melting points were determined in open capillaries in a Gallenkamp apparatus and were uncorrected. The chemical shifts are referenced to the residual not deuterated solvent signal (CHD<sub>2</sub>OD:  $\delta$  (<sup>1</sup>H) = 3.31 ppm,  $\delta$  (<sup>13</sup>C) = 49.86 ppm). The values of the chemical shifts are expressed in ppm, and the coupling constants (*J*) in Hz. An Agilent 1100 LC/MSD operating with an electrospray source was used in mass spectrometry experiments. The purity of compounds **1b–h** was assessed by RP-HPLC (Agilent 1100 series) and was found to be higher than 95% [40]. A Zorbax Eclipse XDB-C8 column (4.6 × 150 mm, 5  $\mu$ m) was used in the HPLC analysis with methanol-H<sub>2</sub>O (0.1% formic acid) (80:20) as the mobile phase at a flow rate of 0.5 mL/min. UV detection was achieved at 280 nm. The absorption spectra were recorded with a PerkinElmer Lambda 900 in the indicated solvent. UV-B irradiations were conducted using a Multyrays chamber equipped with 2 GT15T8 Hg UV-B tubes (2 × 15 Watt) in continuous rotation.

### 6.1. Chemistry

#### 6.1.1. General Procedure for the Synthesis of Compounds **1b–h**

Compounds **1b–h** were prepared by optimizing a previously reported procedure [41]. To a solution, 5-methoxy indanone (1 eq.) in methanol (5 mL/mmol), KOH (1 eq.), and the appropriate aldehyde **4b–h** (1 eq.) were added. The resulting mixture was stirred at room temperature under a nitrogen atmosphere for 2–6 h. Subsequently, the solvent was removed under reduced pressure to obtain a solid residue, which was dissolved in ethyl acetate and washed with brine. The organic phase was dried over anhydrous sodium sulfate, filtered, and concentrated under reduced pressure. The residue was purified by

flash chromatography with the indicated solvent as the eluent to afford an off-white solid corresponding to the desired compound **1b–h** as *E* diastereoisomer. NMR data of the *Z* diastereoisomers of each compound were derived after UV-B light irradiation of the corresponding *E* diastereoisomer until the PSS.

(*E*)-2-(4-((Dimethylamino)methyl)benzylidene)-5-methoxy-2,3-dihydro-1*H*-inden-1-one (**E-1b**).

Compound **E-1b** (0.058 g, yield 53%, m.p. 122–123 °C) was obtained as a pale yellow solid from aldehyde **4b** (0.06 g, 0.36 mmol) after purification with a mixture of ethyl acetate/methanol (9:1) as the eluent. <sup>1</sup>H NMR (400 MHz, CD<sub>3</sub>OD): 2.29 (s, 6H), 3.56 (s, 2H), 3.96 (s, 3H), 4.09 (s, 2H), 7.04 (dd, *J* = 8.6, 2.3, 1H), 7.20 (d, *J* = 2.0, 1H), 7.48 (d, *J* = 8.2, 2H), 7.58 (t, *J* = 2.0, 1H), 7.74 (d, *J* = 8.2, 2H), 7.80 (d, *J* = 8.6, 1H). <sup>13</sup>C NMR (400 MHz, CD<sub>3</sub>OD): 32.0, 43.9, 55.0, 63.2, 109.4, 115.5, 125.5, 129.9, 130.4, 130.6, 132.3, 134.5, 135.4, 139.4, 153.6, 166.1, 193.6. MS(ESI): *m/z* 308.1 [M + H]<sup>+</sup>.

(*Z*)-2-(4-((Dimethylamino)methyl)benzylidene)-5-methoxy-2,3-dihydro-1*H*-inden-1-one (**Z-1b**).

<sup>1</sup>H NMR (400 MHz, CD<sub>3</sub>OD): 2.31 (s, 6H), 3.56 (s, 2H), 3.90 (s, 2H), 3.93 (s, 3H), 7.01 (dd, *J* = 8.6, 2.3, 1H), 7.08 (m, 2H), 7.37 (d, *J* = 8.2, 2H), 7.72 (d, *J* = 8.6, 1H), 8.07 (d, *J* = 8.2, 2H).

(*E*)-2-(4-((Dipropylamino)methyl)benzylidene)-5-methoxy-2,3-dihydro-1*H*-inden-1-one (**E-1c**).

Compound **E-1c** (0.12 g, yield 60%, m.p. 73.5–75.5 °C) was obtained as a pale yellow solid from aldehyde **4c** (0.12 g, 0.55 mmol) after purification with a mixture of petroleum ether/ethyl acetate (1:1) as the eluent. <sup>1</sup>H NMR (400 MHz, CD<sub>3</sub>OD): 0.90 (t, *J* = 7.4, 6H), 1.55 (m, 4H), 2.44 (t, *J* = 7.6, 4H), 3.64 (s, 2H), 3.94 (s, 3H), 4.05 (s, 2H), 7.02 (dd, *J* = 8.5, 2.2, 1H), 7.17 (d, *J* = 2.0, 1H), 7.48 (d, *J* = 8.2, 2H), 7.55 (t, *J* = 1.8, 1H), 7.69 (d, *J* = 8.2, 2H), 7.78 (d, *J* = 8.5, 1H). <sup>13</sup>C NMR (100 MHz, CD<sub>3</sub>OD): 10.8, 19.5, 32.0, 55.0, 55.7, 58.0, 109.4, 115.5, 125.4, 129.4, 130.3, 130.6, 132.6, 134.0, 135.0, 141.4, 153.6, 166.0, 193.7. MS(ESI): *m/z* 364.2 [M + H]<sup>+</sup>.

(*Z*)-2-(4-((Dipropylamino)methyl)benzylidene)-5-methoxy-2,3-dihydro-1*H*-inden-1-one (**Z-1c**).

<sup>1</sup>H NMR (400 MHz, CD<sub>3</sub>OD): 0.91 (t, *J* = 7.4, 6H), 1.55 (m, 4H), 2.46 (t, *J* = 7.6, 4H), 3.65 (s, 2H), 3.90 (s, 2H), 3.93 (s, 3H), 7.01 (dd, *J* = 8.6, 2.2, 1H), 7.08 (m, 2H), 7.38 (d, *J* = 8.2, 2H), 7.72 (d, *J* = 8.7, 1H), 8.06 (d, *J* = 8.2, 2H).

(*E*)-2-(4-((Dibutylamino)methyl)benzylidene)-5-methoxy-2,3-dihydro-1*H*-inden-1-one (**E-1d**).

Compound **E-1d** (0.04 g, yield 64%, m.p. 74.5–75.5 °C) was obtained as a pale yellow solid from aldehyde **4d** (0.04 g, 0.16 mmol) after purification with a mixture of petroleum ether/ethyl acetate (2:1) as the eluent. <sup>1</sup>H NMR (400 MHz, CD<sub>3</sub>OD): 0.93 (t, *J* = 7.3, 6H), 1.34 (m, 4H), 1.52 (m, 4H), 2.48 (t, *J* = 7.5, 4H), 3.64 (s, 2H), 3.95 (s, 3H), 4.08 (s, 2H), 7.03 (dd, *J* = 8.5, 2.2, 1H), 7.19 (d, *J* = 1.9, 1H), 7.48 (d, *J* = 8.1, 2H), 7.56 (s, 1H), 7.70 (d, *J* = 8.2, 2H), 7.79 (d, *J* = 8.6, 1H). <sup>13</sup>C NMR (400 MHz, CD<sub>3</sub>OD): 13.0, 20.3, 28.6, 32.0, 53.3, 55.0, 58.0, 109.4, 115.5, 125.4, 129.5, 130.3, 130.67, 132.6, 134.0, 135.0, 143.6, 153.6, 166.0, 193.7. MS(ESI): *m/z* 392.2 [M + H]<sup>+</sup>.

(*Z*)-2-(4-((Dibutylamino)methyl)benzylidene)-5-methoxy-2,3-dihydro-1*H*-inden-1-one (**Z-1d**).

<sup>1</sup>H NMR (400 MHz, CD<sub>3</sub>OD): 2.31 (s, 6H), 3.56 (s, 2H), 3.90 (s, 2H), 3.93 (s, 3H), 7.01 (dd, *J* = 8.6, 2.3, 1H), 7.08 (m, 2H), 7.37 (d, *J* = 8.2, 2H), 7.72 (d, *J* = 8.6, 1H), 8.07 (d, *J* = 8.2, 2H).

(*E*)-2-(4-((Butyl(methyl)amino)methyl)benzylidene)-5-methoxy-2,3-dihydro-1*H*-inden-1-one (**E-1e**).

Compound **E-1e** (0.071 g, yield 79%, m.p. 62.4–63.0 °C) was obtained as a pale yellow solid from aldehyde **4e** (0.05 g, 0.26 mmol) after purification with a mixture of petroleum ether/ethyl acetate (1:1) as the eluent. <sup>1</sup>H NMR (400 MHz, CD<sub>3</sub>OD): 0.95 (t, *J* = 7.4, 3H), 1.35 (m, 2H), 1.56 (m, 2H), 2.24 (s, 3H), 2.43 (t, *J* = 7.8, 2H), 3.58 (s, 2H), 3.95 (s, 3H), 4.06 (s, 2H), 7.03 (dd, *J* = 8.6, 2.2, 1H), 7.18 (d, *J* = 2.0, 1H), 7.47 (d, *J* = 8.2, 2H), 7.55 (t, *J* = 1.9, 1H), 7.71 (d, *J* = 8.2, 2H), 7.78 (d, *J* = 8.6, 1H). <sup>13</sup>C NMR (100 MHz, CD<sub>3</sub>OD): 12.9, 20.3, 28.8,

32.0, 41.1, 55.0, 56.9, 61.4, 109.4, 115.5, 125.5, 129.8, 130.4, 130.6, 132.4, 134.3, 135.3, 140.0, 153.6, 166.1, 193.6. MS(ESI):  $m/z$  350.2 [M + H]<sup>+</sup>.

(Z)-2-(4-((Butyl(methyl)amino)methyl)benzylidene)-5-methoxy-2,3-dihydro-1H-inden-1-one (Z-1e).

<sup>1</sup>H NMR (400 MHz, CD<sub>3</sub>OD): 0.95 (t,  $J$  = 7.4, 3H), 1.36 (m, 2H), 1.57 (m, 2H), 2.25 (s, 3H), 2.44 (t,  $J$  = 7.8, 2H), 3.59 (s, 2H), 3.90 (s, 2H), 3.93 (s, 3H), 7.01 (dd,  $J$  = 8.6, 2.3, 1H), 7.08 (m, 2H), 7.37 (d,  $J$  = 8.2, 2H), 7.72 (d,  $J$  = 8.6, 1H), 8.07 (d,  $J$  = 8.2, 2H).

(E)-2-(4-((Diisopropylamino)methyl)benzylidene)-5-methoxy-2,3-dihydro-1H-inden-1-one (E-1f).

Compound E-1f (0.022 g, yield 45%, m.p. 74.5–75.5 °C) was obtained as an off-white solid from aldehyde 4f (0.03 g, 0.14 mmol) after purification with a mixture of petroleum ether/ethyl acetate (8:2) as the eluent. <sup>1</sup>H NMR (400 MHz, (CD<sub>3</sub>)<sub>2</sub>CO): 1.07 (d,  $J$  = 6.6, 12H), 3.07 (m, 2H), 3.75 (s, 2H), 3.96 (s, 3H), 4.09 (s, 2H), 7.04 (dd,  $J$  = 8.5, 2.2, 1H), 7.20 (d,  $J$  = 1.9, 1H), 7.50 (t,  $J$  = 2.0, 1H), 7.54 (d,  $J$  = 8.2, 2H), 7.71 (d,  $J$  = 8.2, 2H), 7.75 (d,  $J$  = 8.5, 1H). <sup>1</sup>H NMR (400 MHz, (CD<sub>3</sub>)<sub>2</sub>SO): 1.01 (d,  $J$  = 6.6 Hz, 12H), 3.04–2.87 (m, 2H), 3.67 (s, 2H), 3.90 (s, 3H), 4.07 (s, 2H), 7.04 (dd,  $J$  = 8.5, 2.2 Hz, 1H), 7.19 (d,  $J$  = 1.9 Hz, 1H), 7.44 (s, 1H), 7.48 (d,  $J$  = 8.1 Hz, 1H), 7.69 (d,  $J$  = 8.2 Hz, 1H), 7.72 (t,  $J$  = 6.0 Hz, 1H). <sup>13</sup>C NMR (100 MHz, (CD<sub>3</sub>)<sub>2</sub>SO): 21.1, 32.5, 48.1, 48.7, 56.3, 110.7, 115.9, 125.9, 128.6, 130.9, 131.1, 132.1, 133.6, 135.2, 145.7, 153.4, 165.4, 192.1. MS(ESI):  $m/z$  364.2 [M + H]<sup>+</sup>.

(Z)-2-(4-((Diisopropylamino)methyl)benzylidene)-5-methoxy-2,3-dihydro-1H-inden-1-one (Z-1f).

<sup>1</sup>H NMR (400 MHz, (CD<sub>3</sub>)<sub>2</sub>CO): 1.07 (d,  $J$  = 6.6, 12H), 3.07 (m, 2H), 3.73 (s, 2H), 3.91 (s, 2H), 3.95 (s, 3H), 6.99–7.06 (m, 2H), 7.10 (d,  $J$  = 1.9, 1H), 7.44 (d,  $J$  = 8.2, 2H), 7.71 (d,  $J$  = 8.6, 1H), 8.19 (d,  $J$  = 8.2, 2H).

(E)-2-(4-((Benzyl(methyl)amino)methyl)benzylidene)-5-methoxy-2,3-dihydro-1H-inden-1-one (E-1g).

Compound E-1g (0.055 g, yield 62%, m.p. 126.5–127.5 °C) was obtained as an off-white solid from aldehyde 4g (0.06 g, 0.23 mmol) after purification with a mixture of petroleum ether/ethyl acetate (1:1) as the eluent. <sup>1</sup>H NMR (400 MHz, (CD<sub>3</sub>)<sub>2</sub>CO): 2.19 (s, 3H), 3.58 (s, 2H), 3.60 (s, 2H), 3.96 (s, 3H), 4.10 (s, 2H), 7.04 (dd,  $J$  = 8.5, 2.2, 1H), 7.20 (d,  $J$  = 1.9 Hz, 1H), 7.27 (t,  $J$  = 7.3, 1H), 7.35 (t,  $J$  = 7.5, 2H), 7.43 (d,  $J$  = 7.4, 2H), 7.50 (t,  $J$  = 2.0, 1H), 7.55 (d,  $J$  = 8.1, 2H), 7.75 (d,  $J$  = 8.2, 3H). <sup>1</sup>H NMR (400 MHz, (CD<sub>3</sub>)<sub>2</sub>SO): 2.11 (s, 3H), 3.53 (s, 2H), 3.56 (s, 2H), 3.90 (s, 3H), 4.08 (s, 2H), 7.04 (dd,  $J$  = 8.5, 1.9 Hz, 1H), 7.19 (s, 1H), 7.26 (t,  $J$  = 6.5 Hz, 1H), 7.42–7.30 (m, 4H), 7.45 (s, 1H), 7.49 (d,  $J$  = 8.0 Hz, 2H), 7.74 (m, 3H). <sup>13</sup>C NMR (100 MHz, (CD<sub>3</sub>)<sub>2</sub>SO): 32.5, 42.2, 56.3, 61.1, 61.5, 110.7, 115.9, 125.9, 127.4, 128.7, 129.1, 129.6, 131.1, 131.8, 133.4, 134.2, 135.7, 139.5, 141.5, 153.4, 165.4, 192.1. MS(ESI):  $m/z$  384.2 [M + H]<sup>+</sup>.

(Z)-2-(4-((Benzyl(methyl)amino)methyl)benzylidene)-5-methoxy-2,3-dihydro-1H-inden-1-one (Z-1g).

<sup>1</sup>H NMR (400 MHz, (CD<sub>3</sub>)<sub>2</sub>CO): 2.18 (s, 3H), 3.57 (s, 2H), 3.59 (s, 2H), 3.91 (s, 2H), 3.94 (s, 3H), 7.02 (dd,  $J$  = 8.5, 2.2, 1H), 7.04 (s, 1H), 7.10 (s, 1H), 7.26 (t,  $J$  = 7.3, 1H), 7.35 (t,  $J$  = 7.5, 2H), 7.44 (m, 4H), 7.70 (d,  $J$  = 8.5, 1H), 8.22 (d,  $J$  = 8.2, 2H).

(E)-2-(4-((Benzyl(ethyl)amino)methyl)benzylidene)-5-methoxy-2,3-dihydro-1H-inden-1-one (E-1h).

Compound E-1h (0.06 g, yield 50%, m.p. 118.5–119.5 °C) was obtained as an off-white solid from aldehyde 4h (0.07 g, 0.28 mmol) after purification with a mixture of petroleum ether/ethyl acetate (8:2) as the eluent. <sup>1</sup>H NMR (400 MHz, ((CD<sub>3</sub>)<sub>2</sub>CO): 1.10 (t,  $J$  = 7.1, 3H), 2.53 (q,  $J$  = 7.1, 2H), 3.62 (s, 2H), 3.64 (s, 2H), 3.96 (s, 3H), 4.09 (s, 2H), 7.04 (dd,  $J$  = 8.5, 2.1, 1H), 7.19 (d,  $J$  = 2.0, 1H), 7.25 (t,  $J$  = 7.3, 1H), 7.34 (t,  $J$  = 7.5, 2H), 7.44 (d,  $J$  = 7.4, 2H), 7.49 (s, 1H), 7.55 (d,  $J$  = 8.1, 2H), 7.73 (d,  $J$  = 8.1, 2H), 7.75 (d,  $J$  = 8.2, 1H). <sup>1</sup>H NMR (400 MHz, ((CD<sub>3</sub>)<sub>2</sub>SO): 1.03 (t,  $J$  = 7.1 Hz, 3H), 2.45 (q,  $J$  = 7.1 Hz, 2H), 3.57 (s, 2H), 3.60 (s, 2H), 3.90 (s, 3H), 4.08 (s, 2H), 7.04 (dd,  $J$  = 8.5, 2.3 Hz, 1H), 7.19 (d,  $J$  = 2.0 Hz, 1H), 7.25 (ddd,  $J$  = 8.5, 3.0, 1.5 Hz, 1H), 7.31–7.41 (m, 4H), 7.45 (s, 1H), 7.49 (d,  $J$  = 8.1 Hz, 2H), 7.73 (d,  $J$  = 8.4 Hz, 3H). <sup>13</sup>C NMR (400 MHz, (CD<sub>3</sub>)<sub>2</sub>SO): 12.1, 32.5, 47.0, 56.3, 57.2, 57.5,

110.7, 115.9, 125.9, 127.3, 128.7, 128.9, 129.4, 131.0, 131.1, 131.9, 134.1, 135.6, 140.0, 142.2, 153.4, 165.4, 192.1. MS(ESI):  $m/z$  398.2  $[M + H]^+$ .

(Z)-2-(4-((Benzyl(ethyl)amino)methyl)benzylidene)-5-methoxy-2,3-dihydro-1H-inden-1-one (Z-1h).

$^1\text{H}$  NMR (400 MHz,  $(\text{CD}_3)_2\text{CO}$ ): 1.10 (t,  $J = 7.1$ , 3H), 2.52 (q,  $J = 7.1$ , 2H), 3.61 (s, 2H), 3.63 (s, 2H), 3.91 (s, 2H), 3.94 (s, 3H), 6.99–7.04 (m, 1H), 7.10 (d,  $J = 2.0$ , 1H), 7.24 (t,  $J = 7.3$ , 1H), 7.34 (t,  $J = 7.5$ , 2H), 7.45 (m, 3H), 7.70 (d,  $J = 8.5$ , 1H), 8.21 (d,  $J = 8.2$ , 2H).

#### 6.1.2. General Procedure for the Synthesis of Compounds 6b–h

To a solution of ester 5 (1 equivalent) in dichloromethane (10 mL/mmol), the appropriate secondary amine (3 equivalents) was added. The mixture was stirred at a refluxed temperature for 4–5 h. Then, the solvent was removed under reduced pressure and the resulting oily residue was diluted with dichloromethane and washed with water. The organic phase was dried over anhydrous sodium sulfate, filtered, and concentrated under reduced pressure. The resulting oily residue was purified by flash chromatography using the indicated solvent as the eluent to obtain the desired tertiary amine derivatives 6b–h.

Methyl 4-((dimethylamino)methyl)benzoate (6b) [41]

Compound 6b was obtained as a yellow oil (0.42 g, yield 98%) by using a 1 M solution of dimethyl amine in THF (6.6 mL, 6.60 mmol) after purification with a mixture of petroleum ether/ethyl acetate (1:1) as the eluent.  $^1\text{H}$  NMR (400 MHz,  $\text{CD}_3\text{OD}$ ): 2.28 (s, 6H), 3.57 (s, 2H), 3.92 (s, 3H), 7.46 (d,  $J = 8.4$ , 2H), 8.01 (d,  $J = 8.4$ , 2H). MS(ESI):  $m/z$  194.1  $[M + H]^+$ .

Methyl 4-((dipropylamino)methyl)benzoate (6c) [51]

Compound 6c was obtained as a yellow oil (0.54 g, yield 99%) by using dipropyl amine (0.9 mL, 6.51 mmol) after purification with a mixture of petroleum ether/ethyl acetate (8:2) as the eluent.  $^1\text{H}$  NMR (400 MHz,  $\text{CD}_3\text{OD}$ ): 0.89 (t,  $J = 7.4$ , 6H), 1.53 (m, 4H), 2.43 (t,  $J = 7.5$ , 4H), 3.67 (s, 2H), 3.92 (s, 3H), 7.48 (d,  $J = 8.3$ , 2H), 7.98 (d,  $J = 8.3$ , 2H). MS (ESI):  $m/z$  250.1  $[M + H]^+$ .

Methyl 4-((dibutylamino)methyl)benzoate (6d) [52]

Compound 6d was obtained as a yellow oil (0.59 g, yield 94%) by using dibutyl amine (1.1 mL, 6.81 mmol) after purification with a mixture of petroleum ether/ethyl acetate (9:1) as the eluent.  $^1\text{H}$  NMR (400 MHz,  $\text{CD}_3\text{OD}$ ): 0.91 (t,  $J = 7.3$ , 6H), 1.33 (m, 4H), 1.49 (m, 4H), 2.45 (t,  $J = 7.5$ , 4H), 3.64 (s, 2H), 3.91 (s, 3H), 7.47 (d,  $J = 8.3$ , 2H), 7.98 (d,  $J = 8.3$ , 2H). MS(ESI):  $m/z$  278.2  $[M + H]^+$ .

Methyl 4-((butyl(methyl)amino)methyl)benzoate (6e).

Compound 6e was obtained as a yellow oil (0.51 g, yield 99%) by using N-methylbutan-1-amine (0.8 mL, 6.50 mmol) after purification with a mixture of petroleum ether/ethyl acetate (1:1) as the eluent.  $^1\text{H}$  NMR (400 MHz,  $\text{CD}_3\text{OD}$ ): 0.94 (t,  $J = 7.4$ , 3H), 1.35 (m, 2H), 1.55 (m, 2H), 2.22 (s, 3H), 2.41 (t,  $J = 7.7$ , 2H), 3.59 (s, 2H), 3.92 (s, 3H), 7.46 (d,  $J = 8.1$ , 2H), 8.00 (d,  $J = 8.2$ , 2H).  $^{13}\text{C}$  NMR (100 MHz,  $\text{CD}_3\text{OD}$ ): 13.0, 20.3, 28.9, 41.1, 51.2, 56.9, 61.4, 128.9, 129.1 (two close peaks), 144.0, 167.0. MS(ESI):  $m/z$  236.1  $[M + H]^+$ .

Methyl 4-((diisopropylamino)methyl)benzoate (6f) [53]

Compound 6f was obtained as a yellow oil (0.33 g, yield 60%) by using diisopropyl amine (0.9 mL, 6.53 mmol) after purification with petroleum ether as the eluent.  $^1\text{H}$  NMR (400 MHz,  $\text{CD}_3\text{OD}$ ): 1.08 (d,  $J = 6.6$ , 12H), 3.07 (m, 2H), 3.75 (s, 2H), 3.91 (s, 3H), 7.51 (d,  $J = 8.6$ , 2H), 7.94 (d,  $J = 8.4$ , 2H). MS(ESI):  $m/z$  250.1  $[M + H]^+$ .

Methyl 4-((benzyl(methyl)amino)methyl)benzoate (6g) [54]

Compound 6g was obtained as a yellow oil (0.58 g, yield 99%) by using N-methyl-1-phenylmethanamine (0.8 mL, 6.54 mmol) after purification with a mixture of petroleum ether/ethyl acetate (9:1) as the eluent.  $^1\text{H}$  NMR (400 MHz,  $\text{CD}_3\text{OD}$ ): 2.19 (s, 3H), 3.56 (s, 2H), 3.60 (s, 2H), 3.91 (s, 3H), 7.27 (m, 1H), 7.35 (m, 4H), 7.50 (d,  $J = 8.4$ , 2H), 8.00 (d,  $J = 8.3$ , 2H). MS(ESI):  $m/z$  270.1  $[M + H]^+$ .

Methyl 4-((benzyl(ethyl)amino)methyl)benzoate (6h).

Compound 6h was obtained as a yellow oil (0.61 g, yield 99%) by using N-ethyl-1-phenylmethanamine (1.0 mL, 6.60 mmol) after purification with a mixture of petroleum ether/ethyl acetate (9:1) as the eluent.  $^1\text{H}$  NMR (400 MHz,  $\text{CD}_3\text{OD}$ ): 1.09 (t,  $J = 7.1$ ,

3H), 2.50 (q,  $J = 7.1$ , 2H), 3.57 (s, 2H), 3.62 (s, 2H), 3.90 (s, 3H), 7.23 (t,  $J = 7.2$ , 1H), 7.31 (t,  $J = 7.3$ , 2H), 7.37 (d,  $J = 7.9$ , 2H), 7.48 (d,  $J = 8.1$ , 2H), 7.96 (d,  $J = 8.3$ , 2H).  $^{13}\text{C}$  NMR (100 MHz,  $\text{CD}_3\text{OD}$ ): 10.8, 47.0, 51.1, 57.1, 57.6, 126.6, 127.9, 128.5, 128.6, 128.7, 129.1, 139.2, 145.7, 167.1. MS(ESI):  $m/z$  284.1  $[\text{M} + \text{H}]^+$ .

### 6.1.3. General Procedure for the Synthesis of the Alcohol Derivatives 7b–h

To a solution of the appropriate ester **6b–h** (1 equivalent) in dry THF (5 mL/mmol), a 1 M solution of  $\text{LiAlH}_4$  in THF (1 equivalent) was added. The reaction mixture was stirred at room temperature under a nitrogen atmosphere for 12 h and, subsequently, was concentrated under reduced pressure. The oily residue was dissolved in dichloromethane and then washed with water. The organic phase was dried over anhydrous sodium sulfate, filtered, and concentrated under reduced pressure. The resulting oily residue was purified by flash chromatography using the indicated eluent to obtain the desired alcohol derivatives **7b–h**.

4-((Dimethylamino)methyl)phenylmethanol (**7b**) [55]

Compound **7b** was obtained as a yellow oil (0.37 g, yield 82%) starting from ester **6b** (0.52 g, 2.71 mmol) after purification with ethyl acetate as the eluent.  $^1\text{H}$  NMR (400 MHz,  $\text{CD}_3\text{OD}$ ): 2.26 (s, 6H), 3.49 (s, 2H), 4.63 (s, 2H), 7.34 (m, 4H). MS(ESI):  $m/z$  194.1  $[\text{M} + \text{H}]^+$ .

4-((Dipropylamino)methyl)phenylmethanol (**7c**).

Compound **7c** was obtained as a yellow oil (0.29 g, yield 67%) starting from ester **6c** (0.49 g, 1.98 mmol) after purification with a mixture of petroleum ether/ethyl acetate (8:2) as the eluent.  $^1\text{H}$  NMR (400 MHz,  $\text{CD}_3\text{OD}$ ): 0.88 (t,  $J = 7.4$ , 6H), 1.53 (m, 4H), 2.41 (t,  $J = 7.6$ , 4H), 3.59 (s, 2H), 4.60 (s, 2H), 7.32 (m, 4H).  $^{13}\text{C}$  NMR (100 MHz,  $\text{CD}_3\text{OD}$ ): 10.9, 19.4, 55.5, 57.9, 63.7, 126.6, 129.0, 137.9, 140.1. MS(ESI):  $m/z$  222.2  $[\text{M} + \text{H}]^+$ .

4-((Dibutylamino)methyl)phenylmethanol (**7d**).

Compound **7d** was obtained as a yellow oil (0.16 g, yield 33%) starting from ester **6d** (0.55 g, 1.98 mmol) after purification with a mixture of petroleum ether/ethyl acetate (8:2) as the eluent.  $^1\text{H}$  NMR (400 MHz,  $\text{CD}_3\text{OD}$ ): 0.92 (t,  $J = 7.3$ , 6H), 1.31 (m, 4H), 1.50 (m, 4H), 2.44 (t,  $J = 7.6$ , 4H), 3.59 (s, 2H), 4.61 (s, 2H), 7.32 (m, 4H).  $^{13}\text{C}$  NMR (100 MHz,  $\text{CD}_3\text{OD}$ ): 13.0, 20.3, 28.4, 53.1, 57.9, 63.7, 126.6, 129.0, 137.8, 140.1. MS(ESI):  $m/z$  250.2  $[\text{M} + \text{H}]^+$ .

4-((Butyl(methyl)amino)methyl)phenylmethanol (**7e**).

Compound **7e** was obtained as a yellow oil (0.40 g, yield 83%) starting from ester **6e** (0.55 g, 2.35 mmol) after purification with a mixture of petroleum ether/ethyl acetate (8:2) as the eluent.  $^1\text{H}$  NMR (400 MHz,  $\text{CD}_3\text{OD}$ ): 0.94 (t,  $J = 7.4$ , 3H), 1.34 (m, 2H), 1.54 (m, 2H), 2.21 (s, 3H), 2.40 (t,  $J = 7.8$ , 2H), 3.54 (s, 2H), 4.62 (s, 2H), 7.34 (m, 4H).  $^{13}\text{C}$  NMR (100 MHz,  $\text{CD}_3\text{OD}$ ): 13.0, 20.4, 28.7, 41.0, 56.7, 61.4, 63.6, 126.6, 129.4, 136.5, 140.5. MS(ESI):  $m/z$  208.1  $[\text{M} + \text{H}]^+$ .

4-((Diisopropylamino)methyl)phenylmethanol (**7f**).

Compound **7f** was obtained as a yellow oil (0.09 g, yield 31%) starting from ester **6f** (0.33 g, 1.32 mmol) after purification with a mixture of petroleum ether/ethyl acetate (9:1) as the eluent.  $^1\text{H}$  NMR (400 MHz,  $\text{CD}_3\text{OD}$ ): 1.06 (d,  $J = 6.6$ , 12H), 3.05 (m, 2H), 3.67 (s, 2H), 4.58 (s, 2H), 7.28 (d,  $J = 8.1$ , 2H), 7.36 (d,  $J = 8.2$ , 2H).  $^{13}\text{C}$  NMR (100 MHz,  $\text{CD}_3\text{OD}$ ): 19.7, 47.7 (overlapped to methanol), 48.4, 63.8, 126.5, 127.3, 139.2, 141.9. MS(ESI):  $m/z$  222.1  $[\text{M} + \text{H}]^+$ .

4-((Benzyl(methyl)amino)methyl)phenylmethanol (**7g**).

Compound **7g** was obtained as a yellow oil (0.38 g, yield 80%) starting from ester **6g** (0.53 g, 1.98 mmol) after purification with a mixture of petroleum ether/ethyl acetate (8:2) as the eluent.  $^1\text{H}$  NMR (400 MHz,  $\text{CD}_3\text{OD}$ ): 2.18 (s, 3H), 3.53 (s, 2H), 3.54 (s, 2H), 4.61 (s, 2H), 7.28–7.38 (m, 9H).  $^{13}\text{C}$  NMR (100 MHz,  $\text{CD}_3\text{OD}$ ): 41.0, 61.1, 61.2, 63.6, 126.7, 126.7, 127.9, 129.0, 129.1, 137.3, 138.3, 140.4. MS(ESI):  $m/z$  242.1  $[\text{M} + \text{H}]^+$ .

4-((Benzyl(ethyl)amino)methyl)phenylmethanol (**7h**).

Compound **7h** was obtained as a yellow oil (0.49 g, yield 98%) starting from ester **6h** (0.56 g, 1.98 mmol) after purification with a mixture of petroleum ether/ethyl acetate (8:2) as the eluent.  $^1\text{H}$  NMR (400 MHz,  $\text{CD}_3\text{OD}$ ): 1.09 (t,  $J = 7.1$ , 3H), 2.50 (q,  $J = 7.1$ , 2H), 3.56 (s, 2H), 3.57 (s, 2H), 4.60 (s, 2H), 7.23 (t,  $J = 7.1$ , 1H), 7.33 (m, 8H).  $^{13}\text{C}$  NMR (100 MHz,

CD<sub>3</sub>OD): 10.7, 46.6, 57.1, 57.3, 63.7, 126.6, 126.7, 127.8, 128.7, 128.8, 138.4, 139.3, 140.0. MS(ESI): *m/z* 256.2 [M + H]<sup>+</sup>.

#### 6.1.4. General Procedure for the Synthesis of Aldehyde Derivatives 4b–h

To a solution of the appropriate alcohol derivative 7b–h (1 equivalent) in 1,4-dioxane (3 mL/mmol), MnO<sub>2</sub> (10 equivalents) was added. The reaction mixture was stirred at reflux temperature for 2–4 h and, subsequently, was filtered on celite. The filtrate was concentrated under reduced pressure, and the resulting residue was purified by flash chromatography with the indicated solvent to give the desired aldehyde derivatives 4b–h.

##### 4-((Dimethylamino)methyl)benzaldehyde (4b) [55]

Compound 4b was obtained as a pale yellow oil (0.09 g, yield 24%) starting from alcohol derivative 7b (0.37 g, 2.22 mmol) and was purified using ethyl acetate as the eluent. <sup>1</sup>H NMR (400 MHz, CD<sub>3</sub>OD): 2.26 (s, 6H), 3.58 (s, 2H), 7.56 (d, *J* = 8.1, 2H), 7.91 (d, *J* = 8.2, 2H), 10.0 (s, 1H). MS(ESI): *m/z* 164.1 [M + H]<sup>+</sup>.

##### 4-((Dipropylamino)methyl)benzaldehyde (4c).

Compound 4c was obtained as a pale yellow oil (0.15 g, yield 62%) starting from alcohol derivative 7c (0.25 g, 1.12 mmol) and was purified using a mixture of petroleum ether/ethyl acetate (1:1) as the eluent. <sup>1</sup>H NMR (400 MHz, CD<sub>3</sub>OD): 0.90 (t, *J* = 7.4, 6H), 1.54 (m, 4H), 2.43 (t, *J* = 7.5, 4H), 3.69 (s, 2H), 7.58 (d, *J* = 8.1, 2H), 7.88 (d, *J* = 8.2, 2H), 9.98 (s, 1H). MS(ESI): *m/z* 220.1 [M + H]<sup>+</sup>.

##### 4-((Dibutylamino)methyl)benzaldehyde (4d).

Compound 4d was obtained as a pale yellow oil (0.04 g, yield 36%) starting from alcohol derivative 7d (0.12 g, 0.48 mmol) and was purified using a mixture of petroleum ether/ethyl acetate (2:1) as the eluent. <sup>1</sup>H NMR (400 MHz, CD<sub>3</sub>OD): 0.91 (t, *J* = 7.3, 6H), 1.32 (m, 4H), 1.50 (m, 4H), 2.46 (t, *J* = 7.4, 4H), 3.67 (s, 2H), 7.58 (d, *J* = 8.1, 2H), 7.88 (d, *J* = 8.2, 2H), 9.98 (s, 1H). <sup>13</sup>C NMR (100 MHz, CD<sub>3</sub>OD): 12.9, 20.2, 28.8, 53.5, 58.2, 129.3 (two close peaks), 135.6, 147.5, 192.5. MS(ESI): *m/z* 248.2 [M + H]<sup>+</sup>.

##### 4-((Butyl(methyl)amino)methyl)benzaldehyde (4e).

Compound 4e was obtained as a pale yellow oil (0.78 g, yield 76%) starting from alcohol derivative 7e (1.02 g, 5.02 mmol) and was purified using a mixture of petroleum ether/ethyl acetate (8:2) as the eluent. <sup>1</sup>H NMR (400 MHz, CD<sub>3</sub>OD): 0.94 (t, *J* = 7.4, 3H), 1.36 (m, 2H), 1.55 (m, 2H), 2.23 (s, 3H), 2.42 (t, *J* = 7.6, 2H), 3.61 (s, 2H), 7.57 (d, *J* = 8.0, 2H), 7.90 (d, *J* = 8.2, 2H), 10.00 (s, 1H). <sup>13</sup>C NMR (100 MHz, CD<sub>3</sub>OD): 12.9, 20.2, 28.8, 41.1, 56.9, 60.1, 129.3, 129.7, 137.7, 151.2, 192.5. MS(ESI): *m/z* 206.1 [M + H]<sup>+</sup>.

##### 4-((Diisopropylamino)methyl)benzaldehyde (4f) [56]

Compound 4f was obtained as a pale yellow oil (0.03 g, yield 34%) starting from alcohol derivative 7f (0.09 g, 0.41 mmol) and was purified using a mixture of petroleum ether/ethyl acetate (8:2) as the eluent. <sup>1</sup>H NMR (400 MHz, CD<sub>3</sub>OD): 1.07 (d, *J* = 6.6, 12H), 3.06 (m, 2H), 3.78 (s, 2H), 7.62 (d, *J* = 8.1, 2H), 7.85 (d, *J* = 8.2, 2H), 9.96 (s, 1H). MS(ESI): *m/z* 220.1 [M + H]<sup>+</sup>.

##### 4-((Benzyl(methyl)amino)methyl)benzaldehyde (4g) [57]

Compound 4g was obtained as a pale yellow oil (0.13 g, yield 38%) starting from alcohol derivative 7g (0.34 g, 1.41 mmol) and was purified using a mixture of petroleum ether/ethyl acetate (7:3) as the eluent. <sup>1</sup>H NMR (400 MHz, CD<sub>3</sub>OD): 2.21 (s, 3H), 3.57 (s, 2H), 3.63 (s, 2H), 7.27 (t, *J* = 7.0, 1H), 7.31–7.42 (m, 4H), 7.60 (d, *J* = 8.0, 2H), 7.90 (d, *J* = 8.2, 2H), 9.99 (s, 1H). MS(ESI): *m/z* 240.1 [M + H]<sup>+</sup>.

##### 4-((Benzyl(ethyl)amino)methyl)benzaldehyde (4h) [57]

Compound 4h was obtained as a pale yellow oil (0.07 g, yield 55%) starting from alcohol derivative 7h (0.17 g, 0.87 mmol) and was purified using a mixture of petroleum ether/ethyl acetate (8:2) as the eluent. <sup>1</sup>H NMR (400 MHz, CD<sub>3</sub>OD): 1.11 (t, *J* = 7.1, 3H), 2.53 (q, *J* = 7.1, 2H), 3.60 (s, 2H), 3.67 (s, 2H), 7.24 (t, *J* = 7.2, 1H), 7.35 (t, *J* = 7.5, 2H), 7.38 (m, 2H), 7.61 (d, *J* = 8.1, 2H), 7.88 (d, *J* = 8.2, 2H), 9.97 (s, 1H). MS(ESI): *m/z* 254.1 [M + H]<sup>+</sup>.



### 6.2. Inhibition of Cholinesterases and Monoamine Oxidases

Human isoforms of ChEs (human recombinant AChE and BChE from human serum) and MAOs (from baculovirus-infected insect cells), purchased from Sigma Aldrich (Milan, Italy), were used for inhibition assays. Experiments were performed in 96-well plates (Greiner Bio-One, Kremsmünster, Austria) on the Infinite M1000 Pro plate reader (Tecan, Cernusco s.N., Italy), using already published protocols [46,58–60]. Inhibition data and constants ( $IC_{50}$ s and  $K_i$ s) were calculated with Prism (version 5.01 for Windows; GraphPad Software, San Diego, CA, USA).

The inhibition of human recombinant AChE or BChE from human serum was determined by applying Ellman's spectrophotometric method as described in previously reported protocols [46,59]. Donepezil and tacrine were taken as positive controls in the AChE and BChE inhibition assays, respectively. The reported data agree with those previously reported [40]. The AChE activity was determined in an assay solution containing AChE (0.09 U/mL), 5,50-dithiobis(2-nitrobenzoic acid) (i.e., the Ellman's reagent, 0.33 mM), the test compound (10  $\mu$ M concentration, or seven scalar concentrations for compounds achieving >60% enzyme inhibition at 10  $\mu$ M), in 0.1 M PBS pH 8.0. After 20 min incubation at 25 °C, the substrate acetylthiocholine iodide (5  $\mu$ M) was added, and its hydrolysis rates were monitored for 5.0 min at 412 nm. The BChE inhibitory activity was similarly determined by using BChE (0.09 U/mL) and butyrylthiocholine iodide (5  $\mu$ M) as the substrate.  $IC_{50}$  value, determined by the nonlinear regression method 'log[inhibitor] vs. response', or the % inhibition at 10  $\mu$ M, is expressed as the mean  $\pm$  SD of three independent measurements, each one performed in duplicate. The  $IC_{50}$  values, Michaelis–Menten curve fitting, and inhibition constant ( $K_i$ ) were calculated by nonlinear regression using Prism software.

In MAOs' inhibition assays, each test compound, at 10  $\mu$ M concentration, was preincubated for 20 min at 37 °C with 50  $\mu$ M kynuramine as the substrate in 0.1 M phosphate-buffered solution (PBS) pH 8.0 made 0.39 osmolar with KCl. After the addition of human recombinant MAO-A (250 U/mg) or MAO B (59 U/mg) and a further 30 min of incubation, NaOH was added, and the fluorescence read at 310/400 nm excitation/emission wavelength. For compounds achieving at least 60% inhibition of MAO at 10  $\mu$ M concentration, seven scalar concentrations of each inhibitor were tested, and the concentration producing 50% inhibition of the MAO activity ( $IC_{50}$ ) was calculated by nonlinear regression.  $IC_{50}$  is expressed as mean  $\pm$  SD of three independent measurements, each one performed in duplicate. Clorgiline and safinamide, retested in this work, were taken as positive controls in the MAO A/B assays. For the kinetic study on the inhibition mechanism of MAO B, three diverse scalar concentrations of the inhibitor and seven concentrations of kynuramine were used [40,61,62].

### 6.3. Molecular Docking Calculations

The three-dimensional (3D) structures of hAChE complexed with donepezil (PDB ID: 4EY7) and hMAO-B in complex with safinamide (PDB ID: 2V5Z) were taken from the Protein Data Bank. The protein preparation wizard available in the Schrödinger Suite (Schrödinger Release 2022-4) was employed to optimize X-ray crystal structures: missing side chains have been reconstructed, and protonation states at pH =  $7.4 \pm 0.0$  have been predicted. Finally, energy minimization on the crystal structures was applied using the OPLS\_2005 force field (Banks et al., 2005). Starting from SMILES annotations (Weininger, 1988), 3D structures of *E*-1h and *Z*-1h isomers have been generated, and their protonation states at pH =  $7.4 \pm 0.0$  were computed by LigPrep tool of Schrödinger Suite using the OPLS\_2005 force field. The same steps have been reiterated for hAChE and hMAO-B cognate ligands (i.e., donepezil and safinamide, respectively). Glide v9.1 (Schrödinger Release 2022-4: Glide, Schrödinger, LLC, New York, NY, USA, 2022) was adopted to perform docking simulations upon both targets applying OPLS\_2005 force field. Docking calibration on cognate ligands was carried out in order to find out the most suitable docking protocol for each target: the Root Mean Square Deviation (RMSD) on heavy atoms between the docking pose and the X-ray coordinates of the cognate ligand was computed. In this respect, a

cubic grid box of 15 Å for AChE (RMSD = 0.372) and a cubic grid box of 12 Å for MAO-B (RMSD = 0.467), both placed in the center of mass of the X-ray cognate ligands, were used to perform docking simulations. Standard Precision (SP) docking precision and OPLS\_2005 force field were applied. The top-ranked docking poses of *E*-**1h** and *Z*-**1h** isomers were chosen to examine their target interactions and to compare them with the cognate ligands. All pictures have been made with Pymol (Schrodinger, LLC, 2010. The PyMOL Molecular Graphics System, Version 2.4.0).

## 7. Conclusions

Investigating the AChE/MAO-B dual inhibitory activity of some newly synthesized donepezil-like 2-benzylideneindan-1-one derivatives, which differ for bulkiness/lipophilicity of the unconjugated tertiary amino head, we gathered new clues about the photoswitchable *E/Z* isomerization controlling inhibitors' binding to two AD-related target enzymes. Confirming our previous study [40], all the new compounds were obtained exclusively as *E* geometric isomers. Thanks to the photoswitching properties of the 2-benzylideneindan-1-one chromophore, *Z* isomers were generated in photostationary mixtures (75% of *Z* in all the examined cases) by exposure to UV-B radiation. The pure *E*-isomers showed submicromolar IC<sub>50</sub> values on human AChE, in most cases, with a good selectivity over the BChE isoform. Interestingly, among the donepezil-like molecules synthesized so far, **1h** bearing the *N*-benzyl(ethyl)amino group at the *para* position of the benzylidene moiety proved to be a potent nanomolar AChE inhibitor, achieving an IC<sub>50</sub> of 39 nM (i.e., threefold more potent of the parent *E*-**1a**). The irradiation and consequent enrichment in the *Z* isomer (75% *Z* in the PSS) led to a decrease in activity (IC<sub>50</sub> of PSS-**1h** equals 53 nM), less sharp than that observed with the parent, **1a**. This suggests that the replacement of one ethyl group in *E*-**1a** with a more lipophilic benzyl moiety in *E*-**1h**, due to additional hydrophobic and aromatic interactions with residues into the enzyme binding pockets (e.g., Phe295 as shown by docking calculation), may improve the inhibitory potency of the *E*-**1h** compared to *E*-**1a**, at the same time flattening the differences in IC<sub>50</sub>s between the isomer *E* and the PSS *E/Z* mixture. No other compound showed an increase in inhibitory activity as appreciable as **1h**, whereas the *N*-Me(<sup>*t*</sup>Bu) analog **1e** showed the highest difference in AChE inhibition potency between the thermal steady state *E*-**1e** (IC<sub>50</sub> = 0.102 μM) and the photoinduced one PSS-**1e** (IC<sub>50</sub> = 1.36 μM).

The modifications carried out on the tertiary amino head of the parent compound **1a** seems well-tolerated by MAO-B; indeed, all compounds in the *E* geometry achieved submicromolar IC<sub>50</sub> values and discrete selectivity over MAO-A. The effect of the *E*-to-*Z* photoinduced transition in MAO-B inhibition was more modest (no diastereoselectivity with **1h**) than that observed in AChE. Molecular docking studies performed with the potent dual inhibitor **1h** helped in highlighting the binding modes of the two diastereoisomers in AChE and MAO-B binding sites.

Considering the *in vivo* application limits of ultraviolet radiation (i.e., poor tissue penetrability and potential cytotoxicity), the data discussed herein represent the basis for the optimization of a donepezil-like molecule capable of synergistically inhibiting two target enzymes, namely AChE and MAO-B, involved in neurodegenerative diseases, with the added value of the photomodulation of the pharmacological effect, in order to obtain a tool of interest for the personalized medicine of the future. However, the achievement of the final goal deserves further efforts aimed at improving the characteristics of this family of compounds, paying attention to increasing the wavelength absorption and maintaining (or increasing) the inhibitory potency.

**Supplementary Materials:** The following supporting information can be downloaded at: <https://www.mdpi.com/article/10.3390/molecules28155857/s1>, <sup>1</sup>H NMR spectra of all the compounds and <sup>13</sup>C NMR spectra of the newly synthesized compounds. Additional UV-vis spectra.

**Author Contributions:** Conceptualization, M.P., M.d.C., F.C. and C.D.A.; methodology, M.P., M.d.C., R.P., M.C., M.S., A.C., A.B. and C.M.; software, A.R.T. and O.N.; validation, M.d.C., R.P. and M.C.;

writing—original draft preparation, M.P., M.d.C., A.R.T., O.N., F.C. and C.D.A.; writing—review and editing, all the co-authors; funding acquisition, M.P. and C.D.A. All authors have read and agreed to the published version of the manuscript.

**Funding:** M.P. and M.S. acknowledge the MUR for the financial support under the project ECS0000017 Tuscany-Health Ecosystem—CUP B63C2200068007 spoke 6 for Mission 4 Component 2 (M4C2)—investment 1.5 of the National Recovery and Resilience Plan (PNRR) funded by the European Union “Next Generation EU”. M.d.C., R.P., M.C., and C.D.A. acknowledge the financial support of the Italian Ministry of Education, Universities and Research (PRIN, Grant 201744BN5T\_004).

**Institutional Review Board Statement:** Not applicable.

**Informed Consent Statement:** Not applicable.

**Data Availability Statement:** All data presented in this study are available in the article and in Supplementary Information.

**Conflicts of Interest:** The authors declare no conflict of interest.

**Sample Availability:** Samples of the compounds presented are available from the authors.

## References

1. Available online: <https://www.alzint.org/resource/world-alzheimer-report-2022/> (accessed on 10 March 2023).
2. Gerrow, K.; Triller, A. Synaptic stability and plasticity in a floating world. *Curr. Opin. Neurobiol.* **2010**, *20*, 631–639. [[CrossRef](#)]
3. Finberg, J.P.M.; Rabey, J.M. Inhibitors of MAO-A and MAO-B in Psychiatry and Neurology. *Front. Pharmacol.* **2016**, *7*, 340. [[CrossRef](#)] [[PubMed](#)]
4. Cai, Z. Monoamine oxidase inhibitors: Promising therapeutic agents for Alzheimer’s disease (Review). *Mol. Med. Rep.* **2014**, *9*, 1533–1541. [[CrossRef](#)] [[PubMed](#)]
5. Carradori, S.; Silvestri, R. New Frontiers in Selective Human MAO-B Inhibitors. *J. Med. Chem.* **2015**, *58*, 6717–6732. [[CrossRef](#)]
6. Kumar, B.; Sheetal; Mantha, A.K.; Kumar, V. Recent developments on the structure–activity relationship studies of MAO inhibitors and their role in different neurological disorders. *RSC Adv.* **2016**, *6*, 42660–42683. [[CrossRef](#)]
7. Cereda, E.; Cilia, R.; Canesi, M.; Tesei, S.; Mariani, C.B.; Zecchinelli, A.L.; Pezzoli, G. Efficacy of rasagiline and selegiline in Parkinson’s disease: A head-to-head 3-year retrospective case–control study. *J. Neurol.* **2017**, *264*, 1254–1263. [[CrossRef](#)]
8. Picciotto, M.R.; Higley, M.J.; Mineur, Y.S. Acetylcholine as a Neuromodulator: Cholinergic Signaling Shapes Nervous System Function and Behavior. *Neuron* **2012**, *76*, 116–129. [[CrossRef](#)]
9. Marucci, G.; Buccioni, M.; Dal Ben, D.; Lambertucci, C.; Volpini, R.; Amenta, F. Efficacy of acetylcholinesterase inhibitors in Alzheimer’s disease. *Neuropharmacology* **2021**, *190*, 108352. [[CrossRef](#)]
10. Spencer, C.M.; Noble, S. Rivastigmine. *Drugs Aging* **1998**, *13*, 391–411. [[CrossRef](#)]
11. Dooley, M.; Lamb, H.M. Donepezil. *Drugs Aging* **2000**, *16*, 199–226. [[CrossRef](#)]
12. Maramai, S.; Benchekroun, M.; Gabr, M.T.; Yahiaoui, S. Multitarget Therapeutic Strategies for Alzheimer’s Disease: Review on Emerging Target Combinations. *Biomed Res. Int.* **2020**, *2020*, 5120230. [[CrossRef](#)] [[PubMed](#)]
13. Rullo, M.; Cipolloni, M.; Catto, M.; Colliva, C.; Miniero, D.V.; Latronico, T.; de Candia, M.; Benicchi, T.; Linusson, A.; Giacchè, N.; et al. Probing Fluorinated Motifs onto Dual AChE-MAO-B Inhibitors: Rational Design, Synthesis, Biological Evaluation, and Early-ADME Studies. *J. Med. Chem.* **2022**, *65*, 3962–3977. [[CrossRef](#)] [[PubMed](#)]
14. Mathew, B.; Oh, J.M.; Baty, R.S.; Batiha, G.E.-S.; Parambi, D.G.T.; Gambacorta, N.; Nicolotti, O.; Kim, H. Piperazine-substituted chalcones: A new class of MAO-B, AChE, and BACE-1 inhibitors for the treatment of neurological disorders. *Environ. Sci. Pollut. Res.* **2021**, *28*, 38855–38866. [[CrossRef](#)]
15. Guieu, B.; Lecoutey, C.; Legay, R.; Davis, A.; Sopkova de Oliveira Santos, J.; Altomare, C.D.; Catto, M.; Rochais, C.; Dallemagne, P. First Synthesis of Racemic Trans Propargylamino-Donepezil, a Pleiotrope Agent Able to Both Inhibit AChE and MAO-B, with Potential Interest against Alzheimer’s Disease. *Molecules* **2020**, *26*, 80. [[CrossRef](#)]
16. Benchekroun, M.; Maramai, S. Multitarget-directed ligands for neurodegenerative diseases: Real opportunity or blurry mirage? *Fut. Med. Chem.* **2019**, *11*, 261–263. [[CrossRef](#)] [[PubMed](#)]
17. Ramsay, R.R.; Popovic-Nikolic, M.R.; Nikolic, K.; Uliassi, E.; Bolognesi, M.L. A perspective on multi-target drug discovery and design for complex diseases. *Clin. Transl. Med.* **2018**, *7*, 3. [[CrossRef](#)]
18. Velema, W.A.; Szymanski, W.; Feringa, B.L. Photopharmacology: Beyond Proof of Principle. *J. Am. Chem. Soc.* **2014**, *136*, 2178–2191. [[CrossRef](#)]
19. Duran-Corbera, A.; Catena, J.; Otero-Viñas, M.; Llebaria, A.; Rovira, X. Photoswitchable Antagonists for a Precise Spatiotemporal Control of  $\beta$ 2-Adrenoceptors. *J. Med. Chem.* **2020**, *63*, 8458–8470. [[CrossRef](#)]
20. Fuchter, M.J. On the Promise of Photopharmacology Using Photoswitches: A Medicinal Chemist’s Perspective. *J. Med. Chem.* **2020**, *63*, 11436–11447. [[CrossRef](#)]

21. Rodríguez-Soacha, D.A.; Fender, J.; Ramírez, Y.A.; Collado, J.A.; Muñoz, E.; Maitra, R.; Sotriffer, C.; Lorenz, K.; Decker, M. “Photo-Rimonabant”: Synthesis and Biological Evaluation of Novel Photoswitchable Molecules Derived from Rimonabant Lead to a Highly Selective and Nanomolar “Cis-On” CB1R Antagonist. *ACS Chem. Neurosci.* **2021**, *12*, 1632–1647. [[CrossRef](#)]
22. Qiao, Z.; Fu, W.; Zhang, Y.; Chen, R.; Xu, Z.; Li, Z.; Shao, X. Azobenzene-Semicarbazone Enables Optical Control of Insect Sodium Channels and Behavior. *J. Agric. Food Chem.* **2021**, *69*, 15554–15561. [[CrossRef](#)] [[PubMed](#)]
23. Yue, L.; Pawlowski, M.; Dellal, S.S.; Xie, A.; Feng, F.; Otis, T.S.; Bruzik, K.S.; Qian, H.; Pepperberg, D.R. Robust photoregulation of GABAA receptors by allosteric modulation with a propofol analogue. *Nat. Commun.* **2012**, *3*, 1095. [[CrossRef](#)] [[PubMed](#)]
24. Mourot, A.; Kienzler, M.A.; Banghart, M.R.; Fehrentz, T.; Huber, F.M.E.; Stein, M.; Kramer, R.H.; Trauner, D. Tuning Photochromic Ion Channel Blockers. *ACS Chem. Neurosci.* **2011**, *2*, 536–543. [[CrossRef](#)] [[PubMed](#)]
25. Szymanski, W.; Ourailidou, M.E.; Velema, W.A.; Dekker, F.J.; Feringa, B.L. Light-Controlled Histone Deacetylase (HDAC) Inhibitors: Towards Photopharmacological Chemotherapy. *Chem. A Eur. J.* **2015**, *21*, 16517–16524. [[CrossRef](#)]
26. Reisinger, B.; Kuzmanovic, N.; Löffler, P.; Merkl, R.; König, B.; Sterner, R. Exploiting Protein Symmetry To Design Light-Controllable Enzyme Inhibitors. *Angew. Chem. Int. Ed.* **2014**, *53*, 595–598. [[CrossRef](#)]
27. Rovira, X.; Trapero, A.; Pittolo, S.; Zussy, C.; Faucherre, A.; Jopling, C.; Giraldo, J.; Pin, J.-P.; Gorostiza, P.; Goudet, C.; et al. OptoGluNAM4.1, a Photoswitchable Allosteric Antagonist for Real-Time Control of mGlu4 Receptor Activity. *Cell Chem. Biol.* **2016**, *23*, 929–934. [[CrossRef](#)]
28. Chen, X.; Wehle, S.; Kuzmanovic, N.; Merget, B.; Holzgrabe, U.; König, B.; Sotriffer, C.A.; Decker, M. Acetylcholinesterase Inhibitors with Photoswitchable Inhibition of  $\beta$ -Amyloid Aggregation. *ACS Chem. Neurosci.* **2014**, *5*, 377–389. [[CrossRef](#)]
29. Broichhagen, J.; Jurastow, I.; Iwan, K.; Kummer, W.; Trauner, D. Optical Control of Acetylcholinesterase with a Tacrine Switch. *Angew. Chem. Int. Ed.* **2014**, *53*, 7657–7660. [[CrossRef](#)]
30. Paolino, M.; Gueye, M.; Pieri, E.; Manathunga, M.; Fusi, S.; Cappelli, A.; Latterini, L.; Pannacci, D.; Filatov, M.; Léonard, J.; et al. Design, Synthesis, and Dynamics of a Green Fluorescent Protein Fluorophore Mimic with an Ultrafast Switching Function. *J. Am. Chem. Soc.* **2016**, *138*, 9807–9825. [[CrossRef](#)]
31. Paolino, M.; Giovannini, T.; Manathunga, M.; Latterini, L.; Zampini, G.; Pierron, R.; Léonard, J.; Fusi, S.; Giorgi, G.; Giuliani, G.; et al. On the Transition from a Biomimetic Molecular Switch to a Rotary Molecular Motor. *J. Phys. Chem. Lett.* **2021**, *12*, 3875–3884. [[CrossRef](#)]
32. Tassone, G.; Paolino, M.; Pozzi, C.; Reale, A.; Salvini, L.; Giorgi, G.; Orlandini, M.; Galvagni, F.; Mangani, S.; Yang, X.; et al. Xanthopsin-Like Systems via Site-Specific Click-Functionalization of a Retinoic Acid Binding Protein. *ChemBioChem* **2022**, *23*, e202100449. [[CrossRef](#)] [[PubMed](#)]
33. Gueye, M.; Manathunga, M.; Agathangelou, D.; Orozco, Y.; Paolino, M.; Fusi, S.; Haacke, S.; Olivucci, M.; Léonard, J. Engineering the vibrational coherence of vision into a synthetic molecular device. *Nat. Commun.* **2018**, *9*, 313. [[CrossRef](#)] [[PubMed](#)]
34. Pagano, K.; Paolino, M.; Fusi, S.; Zanirato, V.; Trapella, C.; Giuliani, G.; Cappelli, A.; Zanzoni, S.; Molinari, H.; Ragona, L.; et al. Bile acid binding protein functionalization leads to a fully synthetic rhodopsin mimic. *J. Phys. Chem. Lett.* **2019**, *10*, 2235–2243. [[CrossRef](#)] [[PubMed](#)]
35. Filatov, M.; Paolino, M.; Pierron, R.; Cappelli, A.; Giorgi, G.; Léonard, J.; Huix-Rotllant, M.; Ferré, N.; Yang, X.; Kaliakin, D.; et al. Towards the engineering of a photon-only two-stroke rotary molecular motor. *Nat. Commun.* **2022**, *13*, 6433. [[CrossRef](#)]
36. Paolino, M.; Saletti, M.; Reale, A.; Licciardi, M.; Varvarà, P.; Marquette, A.; Léonard, J.; Bonechi, C.; Donati, A.; Giorgi, G.; et al. Design, Synthesis and Characterization of a Visible-Light-Sensitive Molecular Switch and Its PEGylation towards a Self-Assembling Molecule. *Chem. Eur. J.* **2022**, *28*, e2022014. [[CrossRef](#)]
37. de Candia, M.; Zaetta, G.; Denora, N.; Tricarico, D.; Majellaro, M.; Cellamare, S.; Altomare, C.D. New azepino[4,3-*b*]indole derivatives as nanomolar selective inhibitors of human butyrylcholinesterase showing protective effects against NMDA-induced neurotoxicity. *Eur. J. Med. Chem.* **2017**, *125*, 288–298. [[CrossRef](#)]
38. Purgatorio, R.; de Candia, M.; Catto, M.; Carrieri, A.; Pisani, L.; De Palma, A.; Toma, M.; Ivanova, O.A.; Voskressensky, L.G.; Altomare, C.D. Investigating 1,2,3,4,5,6-hexahydroazepino[4,3-*b*]indole as scaffold of butyrylcholinesterase-selective inhibitors with additional neuroprotective activities for Alzheimer’s disease. *Eur. J. Med. Chem.* **2019**, *177*, 414–424. [[CrossRef](#)]
39. Purgatorio, R.; Gambacorta, N.; de Candia, M.; Catto, M.; Rullo, M.; Pisani, L.; Nicolotti, O.; Altomare, C.D. First-in-Class Isonipecotamide-Based Thrombin and Cholinesterase Dual Inhibitors with Potential for Alzheimer Disease. *Molecules* **2021**, *26*, 5208. [[CrossRef](#)]
40. Paolino, M.; Rullo, M.; Maramai, S.; de Candia, M.; Pisani, L.; Catto, M.; Mugnaini, C.; Brizzi, A.; Cappelli, A.; Olivucci, M.; et al. Design, synthesis and biological evaluation of light-driven on-off multitarget AChE and MAO-B inhibitors. *RSC Med. Chem.* **2022**, *13*, 873–883. [[CrossRef](#)]
41. Sheng, R.; Xu, Y.; Hu, C.; Zhang, J.; Lin, X.; Li, J.; Yang, B.; He, Q.; Hu, Y. Design, synthesis and AChE inhibitory activity of indanone and aurone derivatives. *Eur. J. Med. Chem.* **2009**, *44*, 7–17. [[CrossRef](#)]
42. Petermayer, C.; Thumser, S.; Kink, F.; Mayer, P.; Dube, H. Hemiindigo: Highly bistable photoswitching at the biooptical window. *J. Am. Chem. Soc.* **2017**, *139*, 15060–15067. [[CrossRef](#)] [[PubMed](#)]
43. Lazinski, L.M.; Royal, G.; Robin, M.; Maresca, M.; Haudecoeur, R. Bioactive aurones, indanones, and other hemiindigoid scaffolds: Medicinal chemistry and photopharmacology perspectives. *J. Med. Chem.* **2022**, *65*, 12594–12625. [[CrossRef](#)] [[PubMed](#)]

44. Salum, M.L.; Arroyo Mañez, P.; Luque, F.J.; Erra-Balsells, R. Combined experimental and computational investigation of the absorption spectra of E- and Z-cinnamic acids in solution: The peculiarity of Z-cinnamics. *J. Photochem. Photobiol. B Biol.* **2015**, *148*, 128–135. [[CrossRef](#)] [[PubMed](#)]
45. Purgatorio, R.; de Candia, M.; Catto, M.; Rullo, M.; Pisani, L.; Denora, N.; Carrieri, A.; Nevskaya, A.A.; Voskressensky, L.G.; Altomare, C.D. Evaluation of Water-Soluble Mannich Base Prodrugs of 2,3,4,5-Tetrahydroazepino[4,3-b]indol-1(6H)-one as Multitarget-Directed Agents for Alzheimer's Disease. *ChemMedChem* **2021**, *16*, 589–598. [[CrossRef](#)]
46. Purgatorio, R.; Gambacorta, N.; Samarelli, F.; Lopopolo, G.; de Candia, M.; Catto, M.; Nicolotti, O.; Altomare, C.D. Assessing the Role of a Malonamide Linker in the Design of Potent Dual Inhibitors of Factor Xa and Cholinesterases. *Molecules* **2022**, *27*, 4269. [[CrossRef](#)]
47. Nel, M.S.; Petzer, A.; Petzer, J.P.; Legoabe, L.J. 2-Benzylidene-1-indanone derivatives as inhibitors of monoamine oxidase. *Bioorg. Med. Chem. Lett.* **2016**, *26*, 4599–4605. [[CrossRef](#)]
48. Affini, A.; Hagenow, S.; Zivkovic, A.; Marco-Contelles, J.; Stark, H. Novel indanone derivatives as MAO-B/H3R dual-targeting ligands for treatment of Parkinson's disease. *Eur. J. Med. Chem.* **2018**, *148*, 487–497. [[CrossRef](#)]
49. Pourshojaei, Y.; Abiri, A.; Eskandari, K.; Haghighijoo, Z.; Edraki, N.; Asadipour, A. Phenoxyethyl Piperidine/Morpholine Derivatives as PAS and CAS Inhibitors of Cholinesterases: Insights for Future Drug Design. *Sci. Rep.* **2019**, *9*, 19855. [[CrossRef](#)]
50. Alagöz, M.A.; Oh, J.M.; Zenni, Y.N.; Özdemir, Z.; Abdelgawad, M.A.; Naguib, I.A.; Ghoneim, M.M.; Gambacorta, N.; Nicolotti, O.; Kim, H.; et al. Development of a Novel Class of Pyridazinone Derivatives as Selective MAO-B Inhibitors. *Molecules* **2022**, *27*, 3801. [[CrossRef](#)]
51. Jaafar, H.; Li, H.; Misal Castro, L.C.; Zheng, J.; Roisnel, T.; Dorcet, V.; Sortais, J.-B.; Darcel, C. Phosphane-Pyridine Iron Complexes: Synthesis, Characterization and Application in Reductive Amination through the Hydrosilylation Reaction. *Eur. J. Inorg. Chem.* **2012**, *2012*, 3546–3550. [[CrossRef](#)]
52. Kuwano, R.; Kondo, Y.; Matsuyama, Y. Palladium-Catalyzed Nucleophilic Benzylic Substitutions of Benzylic Esters. *J. Am. Chem. Soc.* **2003**, *125*, 12104–12105. [[CrossRef](#)] [[PubMed](#)]
53. Das, S.; Karmakar, H.; Bhattacharjee, J.; Panda, T.K. Aluminium complex as an efficient catalyst for the chemo-selective reduction of amides to amines. *Dalton Trans.* **2019**, *48*, 11978–11984. [[CrossRef](#)] [[PubMed](#)]
54. Lator, A.; Gaignard Gaillard, Q.; Mérel, D.S.; Lohier, J.-F.; Gaillard, S.; Poater, A.; Renaud, J.-L. Room-Temperature Chemoselective Reductive Alkylation of Amines Catalyzed by a Well-Defined Iron(II) Complex Using Hydrogen. *J. Org. Chem.* **2019**, *84*, 6813–6829. [[CrossRef](#)] [[PubMed](#)]
55. Horiuchi, T.; Nagata, M.; Kitagawa, M.; Akahane, K.; Uoto, K. Discovery of novel thieno[2,3-d]pyrimidin-4-yl hydrazone-based inhibitors of cyclin D1-CDK4: Synthesis, biological evaluation and structure-activity relationships. Part 2. *Bioorg. Med. Chem.* **2009**, *17*, 7850–7860. [[CrossRef](#)]
56. Claffey, J.; Müller-Bunz, H.; Tacke, M. Benzyl-substituted titanocene dichloride anticancer drugs: From lead to hit. *J. Organometal. Chem.* **2010**, *695*, 2105–2117. [[CrossRef](#)]
57. Rizzo, S.; Bartolini, M.; Ceccarini, L.; Piazza, L.; Gobbi, S.; Cavalli, A.; Recanatini, M.; Andrisano, V.; Rampa, A. Targeting Alzheimer's disease: Novel indanone hybrids bearing a pharmacophoric fragment of AP2238. *Bioorg. Med. Chem.* **2010**, *18*, 1749–1760. [[CrossRef](#)]
58. Purgatorio, R.; de Candia, M.; De Palma, A.; De Santis, F.; Pisani, L.; Campagna, F.; Cellamare, S.; Altomare, C.D.; Catto, M. Insights into Structure-Activity Relationships of 3-Arylhydrazonoindolin-2-One Derivatives for Their Multitarget Activity on  $\beta$ -Amyloid Aggregation and Neurotoxicity. *Molecules* **2018**, *23*, 1544. [[CrossRef](#)]
59. Purgatorio, R.; Kulikova, L.N.; Pisani, L.; Catto, M.; Candia, M.; Carrieri, A.; Cellamare, S.; De Palma, A.; Beloglazkin, A.A.; Reza Raesi, G.; et al. Scouting around 1,2,3,4-tetrahydrochromeno[3,2-c]pyridin-10-ones for single- and multitarget ligands directed towards relevant Alzheimer's targets. *ChemMedChem* **2020**, *15*, 1947–1955. [[CrossRef](#)]
60. Titov, A.A.; Purgatorio, R.; Obydennik, A.Y.; Listratova, A.V.; Borisova, T.N.; de Candia, M.; Catto, M.; Altomare, C.D.; Varlamov, A.V.; Voskressensky, L.G. Synthesis of isomeric 3-Benzazecines decorated with endocyclic allene moiety and exocyclic conjugated double bond and evaluation of their anticholinesterase activity. *Molecules* **2022**, *27*, 6276. [[CrossRef](#)]
61. Kulikova, L.N.; Purgatorio, R.; Beloglazkin, A.A.; Tafeenko, V.A.; Reza, R.G.; Levickaya, D.D.; Sblano, S.; Boccarelli, A.; de Candia, M.; Catto, M.; et al. Chemical and Biological Evaluation of Novel 1H-Chromeno[3,2-c]pyridine Derivatives as MAO Inhibitors Endowed with Potential Anticancer Activity. *Int. J. Mol. Sci.* **2023**, *24*, 7724. [[CrossRef](#)]
62. Kulikova, L.N.; Raesi, G.R.; Levickaya, D.D.; Purgatorio, R.; Spada, G.; Catto, M.; Altomare, C.D.; Voskressensky, L.G. Synthesis of Novel Benzo[b][1,6]naphthyridine Derivatives and Investigation of Their Potential as Scaffolds of MAO Inhibitors. *Molecules* **2023**, *28*, 1662. [[CrossRef](#)] [[PubMed](#)]

**Disclaimer/Publisher's Note:** The statements, opinions and data contained in all publications are solely those of the individual author(s) and contributor(s) and not of MDPI and/or the editor(s). MDPI and/or the editor(s) disclaim responsibility for any injury to people or property resulting from any ideas, methods, instructions or products referred to in the content.